2000

A closer look at remanence-dominated aeromagnetic anomalies: Rock magnetic properties and magnetic mineralogy of the Russell Belt microcline-sillimanite gneiss, northwest Adirondack Mountains, New York

Laurie Brown, *University of Massachusetts - Amherst*
S. A McEnroe

JOURNAL OF GEOPHYSICAL RESEARCH, VOL. 105, NO. B7, PAGES 16,437–16,456, JULY 10, 2000

A closer look at remanence-dominated aeromagnetic anomalies: Rock magnetic properties and magnetic mineralogy of the Russell Belt microcline-sillimanite gneiss, northwest Adirondack Mountains, New York

Suzanne A. McEnroe

Norwegian Geological Survey, Trondheim, Norway

Laurie L. Brown

Department of Geosciences, University of Massachusetts, Amherst

Abstract. A large, distinct negative aeromagnetic anomaly of over 2000 nT associated with microcline-sillimanite-quartz gneisses in the Russell area, northwest Adirondack Mountains, was previously shown to be remanence-dominated, although the carriers of remanence were not well documented. Russell Belt gneisses have a strong natural remanent magnetization with steep remanence directions, D = 263°, I = -58°, an average intensity of 3.6 A/m, and typical susceptibilities of 10^{-4} SI. The remanence is thermochemical in origin, acquired during cooling from peak metamorphic conditions of 650°-750°C during the Ottawan Orogen (1050-1080 Ma). The reversed polarity of remanence reflects a reversed paleofield, rather than self-reversed, contrary to earlier suggestions. The gneisses contain up to 3% oxide, predominantly metamorphic titanohematite, which accounts for the low susceptibility values and highly stable remanence. Optical observations show titanohematite grains with multiple generations of ilmenite, pyrophanite, rutile, and spinel exsolution lamellae. Microprobe analyses confirm titanohematite compositions ranging from 72 to 97% Fe_2O_3, with $hematite_{83}$ being most typical. In rare samples, inclusions of magnetite were identified. The ubiquitous presence of titanohematite, and the rare occurrence of magnetite, is supported by thermal and alternating field demagnetization studies, saturation magnetization measurements, hysteresis properties, temperature-hysteresis studies, and low-temperature remanence measurements. Numerous crustal granulites have titanohematite as part of the oxide assemblage, and this may contribute a strong remanent component to what have previously been considered to be solely induced anomalies.

1. Introduction

The collection of magnetic data from fixed-wing aircraft has been employed as a geophysical exploration tool for over 50 years. The presence of both short- and long- wavelength anomalies has been attributed primarily to induced magnetization in basement or deep crustal rocks. Although some interest in the contribution of remanent magnetization to observed anomalies has been voiced in the past [*Green*, 1960; *Books*, 1962; *Watkins*, 1961], remanent magnetization is now usually ignored [*Shive et al.*, 1992]. In a few cases, remanent magnetization is discussed for isolated short-wavelength anomalies [*Rajagopalan et al.*, 1995; *Kelso et al.*, 1993] but only rarely for long-wavelength observations [*Kelso et al.*, 1993; *Kletetschka and Stout*, 1998; *McEnroe*, 1995; *McEnroe et al.*, 2000]. In fact, *Shive* [1989a,b] argues against the possibility that either stable or viscous remanent magnetization contributes substantially to deep crustal anomalies, although the importance of single-domain magnetite grains should not be overlooked [*Worm*, 1989].

In addition, the mineralogical cause of the induced magnetization is almost always assumed to be magnetite [*Shive et al.*, 1992], although *Grant* [1985] does acknowledge the importance of other oxides, particularly the titanohematite series. Specifically dealing with granulite-facies rocks, representative of material in the deep crust, the interpretation is the same, with magnetite seen as the dominant mineral and magnetization being entirely induced [*Schlinger*, 1985; *Mayhew et al.*, 1991]. Twenty years ago, *Reford* [1980] voiced the concern that rock magnetic studies are ignored in aeromagnetic interpretation, and in general, one finds that this concern is still true [*Blakely*, 1996; *Clark*, 1997]. All too commonly, a simple homogenous body of rock of uniform magnetization is assumed to be the cause of observed anomalies and is used in detailed modeling.

Paper number 2000JB900051
0148-0227/00/2000JB900051$09.00

Although the ambiguities of potential field modeling are great, tight constraints on models can only be produced if detailed magnetic properties are known. The possibility that a strong negative remanence influences the resulting anomaly is often evident; strong positive remanence is often not so easily identified [*McEnroe et al.*, 1996]. Understanding the basic rock magnetic properties of source rocks is particularly important with the new high-resolution aeromagnetic techniques employed today [*Clark*, 1997, 1999] because they contribute important control on the reliability of magnetic models. With greater development of petrophyical databases, coupled with an increased understanding of the relationship between magnetic mineralogy and magnetic anomalies, we should be able to refine interpretation of long-wavelength anomalies from satellite studies.

In this paper we deal with a pronounced negative aeromagnetic anomaly from the Grenville terrane of the Adirondack Mountains, New York. We will establish the compositions and magnetic characteristics of the oxide minerals causing the magnetic anomaly. The foundation of our petrologic and mineralogical research is the extensive work by *Buddington* [1939] (and later work) on these rocks as part of his larger research program in the Adirondack Mountains and his collaboration with J. R. Balsley to investigate their magnetic properties. In a series of excellent and detailed mineralogical, petrological, and geophysical works they showed that titanohematite is the dominant oxide, and magnetite is apparently not part of the assemblage at this locality [*Balsley and Buddington*, 1954, 1957, 1958]. Therefore, in addition to analyzing for titanohematite we designed our rock magnetic experiments to search specifically for a fine- to ultra fine-grained magnetite.

2. Geological Setting

The Adirondack Mountains consist of high-grade Mid-Proterozoic gneisses, marbles and schists that form the southeast extension of the Grenville Province of Ontario and Quebec, all of which were metamorphosed and deformed 1300 to 1000 Ma [*Mezger et al.*, 1991; *McLelland et al.*, 1996]. Unlike Grenville basement exposed in the Appalachians to the east, the Adirondacks have not suffered any significant Paleozoic metamorphism and thus represent mineral assemblages and structural configurations related to the Grenville orogenic cycle [*Wiener et al.*, 1984; *McLelland et al.*, 1996]. The Adirondacks are divided into the Highland province, composed mostly of granulite-facies metamorphosed igneous rocks including a large amount of anorthosite, and the Lowlands province, dominated by metamorphosed sedimentary and volcanic rocks of amphibolite facies. These correspond to the Central Granulite terrane and Central Metasedimentary terrane of the Grenville Province in Canada. A distinct zone of intensely deformed rocks referred to as the Carthage-Colton mylonite zone (CCMZ) lies near the boundary of these two regions [*Wiener et al.*, 1984; *Mezger et al.*, 1992] (Figure 1). Metamorphic conditions for all of the Highlands reached granulite grade, with peak metamorphic temperatures of 650°C to 775°C and pressures of up to 8 kbar [*Bohlen et al.*, 1985; *Spear and Markussen*, 1997]. An angular unconformity separates the Adirondack basement from the Upper Cambrian Potsdam Sandstone and overlying Cambro-Ordovician strata [*McLelland*, 1993].

The northwest Adirondacks have been studied for some time, particularly as part of strategic mineral exploration [*Buddington and Leonard*, 1962]. The samples discussed in this paper are from microcline gneisses, commonly sillimanitic, locally garnetiferous, and commonly associated with metamorphosed sedimentary layers. They are located just southeast of the CCMZ in the Highland province. Recent mapping and synthesis in the area has included these rocks within the Baldface Hill Gneiss [*Wiener et al.*, 1984]. This unit has been interpreted to represent sedimentary and felsic volcanic rocks found discontinuously on either side of the CCMZ that were metamorphosed to granulite facies. Five phases of deformation have been recognized in the northwest Adirondacks, including isoclinal nappes and upright to overturned NE directed folds and associated amphibolite to granulite facies metamorphism [*Wiener et al.*, 1984]. Although some of these sillimanite-microcline gneisses are rich in magnetite ± ilmenite to the extent of being mined for iron ore [*Leonard and Buddington*, 1962], other parts of the unit are virtually magnetite-free with titanohematite ± ilmenite and rutile as the dominant oxides [*Balsley and Buddington*, 1954, 1958].

Samples for this study were collected in the area south of Russell, New York (44.43°N, 75.15°W), in the "Russell Belt" described by *Balsley and Buddington* [1954]. Original field notes of Buddington were used to relocate outcrops with known mineralogical and magnetic behavior. At each of six sites (Figure 1), samples were drilled and oriented in the field or drilled from oriented blocks collected at the outcrops and returned to the lab. Due to the extremely heterogeneous nature of these rocks, a number of cores at each site were collected to ensure that a range of compositions was sampled.

3. Russell Belt Magnetic Anomaly

Some of the first aeromagnetic data ever collected were from the Adirondack Mountains, as part of the U. S. Geological Survey's Strategic Minerals Program, here explicitly looking for magnetite deposits. A survey encompassing Russell and areas to the east [*Balsley*, 1954] covered over 6,100 square miles, and was flown at an altitude of 1000 ft with a 1/4-mile line spacing. Very striking positive anomalies, as to be expected from magnetite-rich rocks with high induced magnetization, were found, and many were later shown to be associated with ore bodies. In addition, several strong negative anomalies, unrelated to induced signals, were evident, including one over the Russell Belt (Figure 1). *Balsley and Buddington* [1954, 1957; 1958] recognized that these anomalies were unusual, and they combined oxide petrography, rock and mineral chemistry, and susceptibility and natural remanent magnetization (NRM) measurements in an attempt to interpret them.

The Russell Belt negative aeromagnetic anomaly is ~ 15 km long and 3 km wide, with an amplitude of over 2000 nT. Although there are numerous other anomalies in the region, there is no indication that this negative

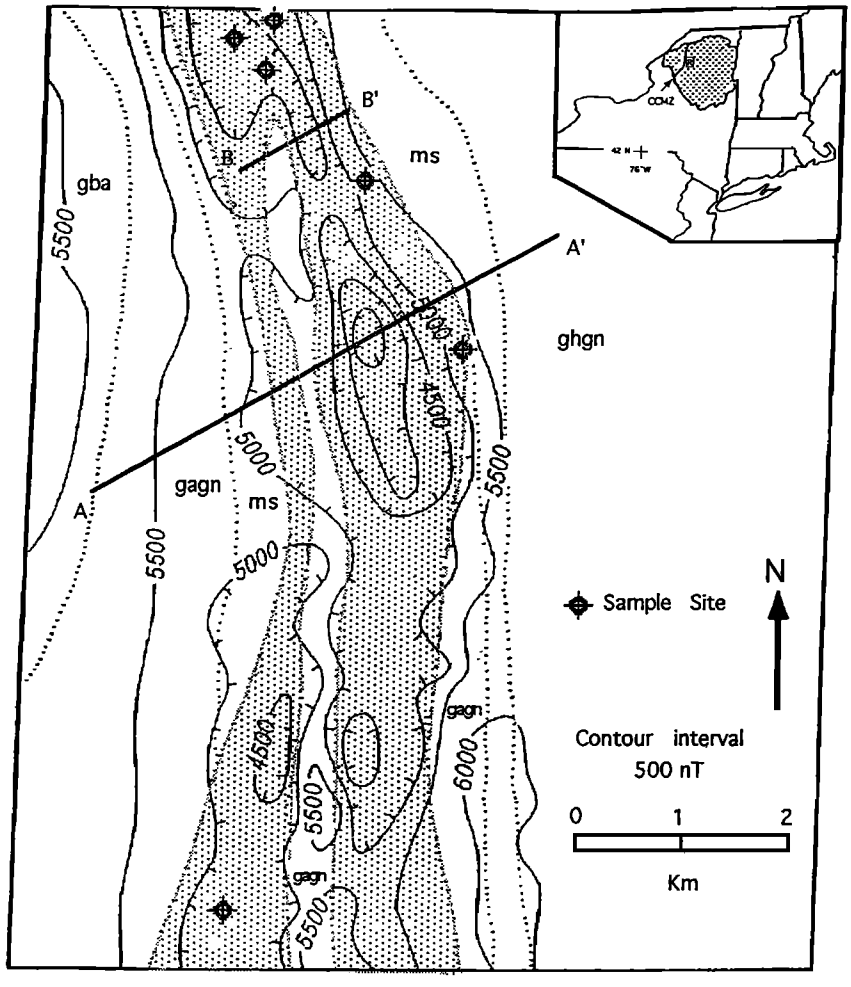

Figure 1. Simplified geologic and aeromagnetic anomaly map of part of the Russell Belt, northwest Adirondacks. Stippled unit (gms) is microcline granite gneiss with associated metasedimentary layers; gagn, alaskite gneiss; gba, anorthosite gabbro gneiss; ghgn, hornblende-microcline-oligoclase granite gneiss; ms, metasedimentary rocks and related migmatites. Sample sites used in this paper are shown by circled crosses. AA' is location of aeromagnetic profile shown in Figure 2a. BB' is location of ground magnetic profile shown in Figure 2b. Adapted from *Balsley and Buddington* [1958] and *Buddington and Leonard* [1962]. Inset shows location of Adirondack Mountains (stippled area), CCMZ is Carthage-Colton mylonite zone, shown by solid line. Box shows location of the Russell belt. Contour interval is 500 nT.

anomaly is paired with or related to any of the positive anomalies. The local geomagnetic field in the northwest Adirondacks currently has a declination of 347°, inclination of 73°, and magnitude of 58,000 nT. Given these parameters, the observed anomaly cannot be produced by induced magnetization alone. A profile taken from the detailed aeromagnetic anomaly map [*Balsley*, 1954] is shown on Figure 2a. The steep gradients of the anomaly indicate that the source materials lie at or near the surface. *Balsley and Buddington* [1954] related the anomaly to the microcline granite gneisses (unit "gms" on Figure 1) and concluded that the negative sense of the anomaly was determined by a strong negative remanent magnetization of these rocks. Because at the time there was little knowledge of geomagnetic field reversals, they surmised that the negative directions might be due to self-reversals, as proposed by *Néel* [1951].

We collected ground magnetic data with a proton precession magnetometer across the widest part of the anomaly near south Russell, along line BB' of Figure 1, using a 15-foot (4.6m) spacing (Figure 2b). The data are corrected to the average value of 58,000 nT, the current magnetic field in the area. This traverse covers the region of the lowest part of the aeromagnetic anomaly and shows considerable variation over a short distance. Although the collected data do not extend outside of the mapped regions of unit gms in this area, they still indicate a large variable negative magnetic anomaly with nearly 4000 nT of relief over a confined area. These results confirm that the anomalies are due to rocks at the surface with highly variable magnetization.

4. Magnetic Mineralogy

The magnetic and chemical properties of members of the ilmenite ($FeTiO_3$) - hematite (Fe_2O_3) solid solution series are of interest here because titanohematite is the dominant oxide in the Russell Belt gneiss [*Balsley and Buddington*, 1958]. This solid solution contains both

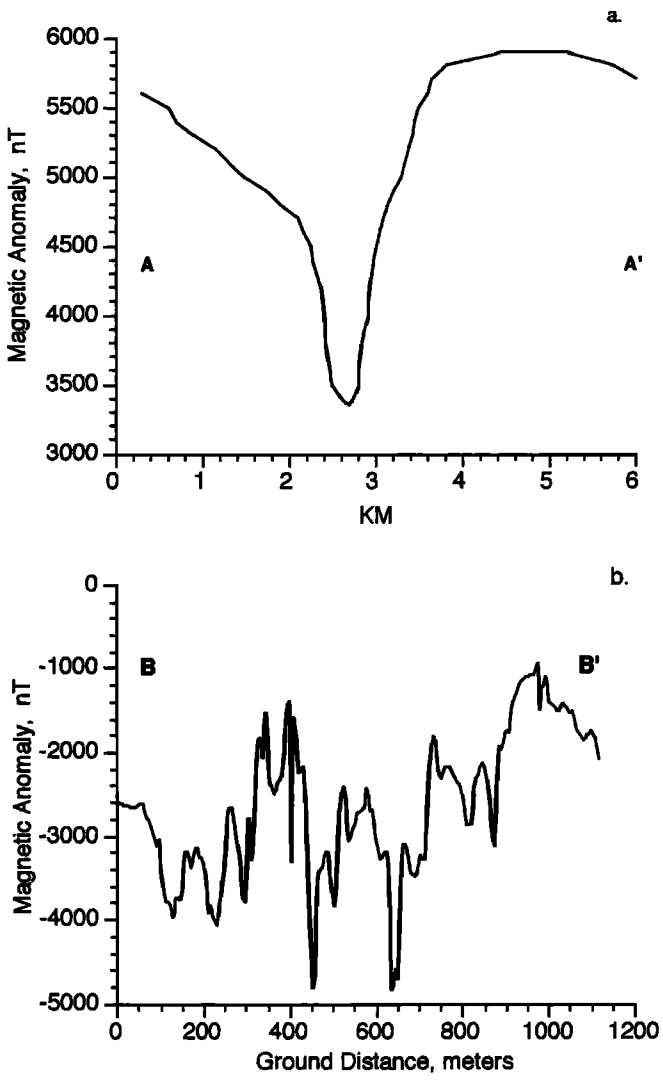

Figure 2. Magnetic anomalies in the Russell Belt. (a) Aeromagnetic anomaly profile along line AA' of Figure 1, taken from the detailed anomaly map of *Balsley* [1954]; arbitrary datum level. (b) Ground magnetic anomaly profile from data collected along line BB' in Figure 1, values relative to datum level of present magnetic field intensity of 58,000 nT.

antiferromagnetic and ferrimagnetic members. Early investigations of the magnetic properties of this series [*Bozorth et al.*, 1957; *Ishikawa and Akimoto*, 1957, 1958a, b; *Ishikawa*, 1958; *Uyeda*, 1958; *Westcott-Lewis and Parry*, 1971a, b] were mostly made on synthetic samples, but a few studies included natural samples. The end-member hematite and hematite-rich $R\bar{3}c$ structures give rise only to a weak antiferromagnetic moment, with a saturation magnetization of 2.5 kA/m for end-member hematite [*Thompson and Oldfield*, 1986] but somewhat higher values for hematite$_{80\text{-}90}$ [*Bozorth et al.*, 1957]. Conversely, compositions between ilmenite$_{50\text{-}85}$ with Ti-ordered $R\bar{3}$ structures, are ferrimagnetic, with a high saturation magnetization but low Néel temperatures. Rapidly chilled members in this composition range have intriguing magnetic properties, one of which is the ability to acquire a self-reversed thermoremanent magnetization [*Nagata et al.*, 1952; *Hoffman*, 1992; *Nord and Lawson*, 1989, 1992]. Known examples of ilmenite with a high saturation magnetization, strong self-reversed magnetization and a strong phase coupling [*Ishikawa and Syono*, 1963] are from rapidly chilled volcanic rocks. Such conditions would be highly unlikely in a slowly cooled terrane such as the Adirondack Mountains, where extensively exsolved phases occur due to the long cooling history.

Representative specimens were examined in polished thin section, both in reflected and transmitted light. In reflected light, detailed observations could be made on multidomain (MD) to single-domain size (SD) oxide and sulfide minerals. Because hematite has a broad SD-size range, up to 15 μm [*Dunlop and Özdemir*, 1997], it is easy to observe SD to MD phases optically. Given the large range in magnetic properties of the hematite-ilmenite solid solution series described above, compositional data were collected on selected polished sections on a Cameca electron microprobe at the University of Massachusetts, Amherst.

The principal silicates in the Russell Gneiss are quartz, plagioclase, microcline, sillimanite, ± garnet, muscovite, and biotite. There is secondary chlorite partially or completely replacing biotite, and the plagioclase is commonly sericitized. In reflected light, samples contain up to 3% well-crystallized SD to MD size subhedral titanohematite grains with abundant and complex exsolution features. A small amount of secondary magnetite, ilmenite or hematite can be found in the biotite and in cross fractures in sillimanite. The Russell Gneiss has an overall resemblance to granitoid intrusive rocks metamorphosed to upper amphibolite or granulite facies, which suffered minor late or post metamorphic hydrothermal alteration, but there are features arguing against this interpretation: (1) The rocks are layered, with common and abrupt changes in composition. (2) Large amounts of muscovite and sillimanite in many layers indicate bulk compositions outside any common igneous protolith. (3) The dominance of titanohematite in the oxides and other features of a highly variable opaque mineralogy suggest extremely oxidized protolith compositions completely outside the normal igneous realm. Our best explanation for this combination of features is that the protolith of the Russell Gneiss was a sequence of felsic volcanics or volcanic-sedimentary rocks that underwent strong and variable hydrothermal alteration including alkali leaching and oxidation, most probably during original Meso-Proterozoic deposition. These processes produced highly variable aluminous and oxidized bulk compositions, which in turn produced unusual mineral assemblages, particularly the opaque oxide assemblages, during Grenville regional metamorphism.

Titanohematite grains have abundant exsolution features (Figures 3a-3g). Fine ilmenite exsolution lamellae parallel to {0001} are common and some contain very-fine rutile lamellae. Second generation ilmenite lamellae, also parallel to {0001}, are common. Subsequent generations of hematite and ilmenite lamellae are at or below the limits of optical resolution, and some hematite lamellae may be below the single-domain to superparamagnetic transition.

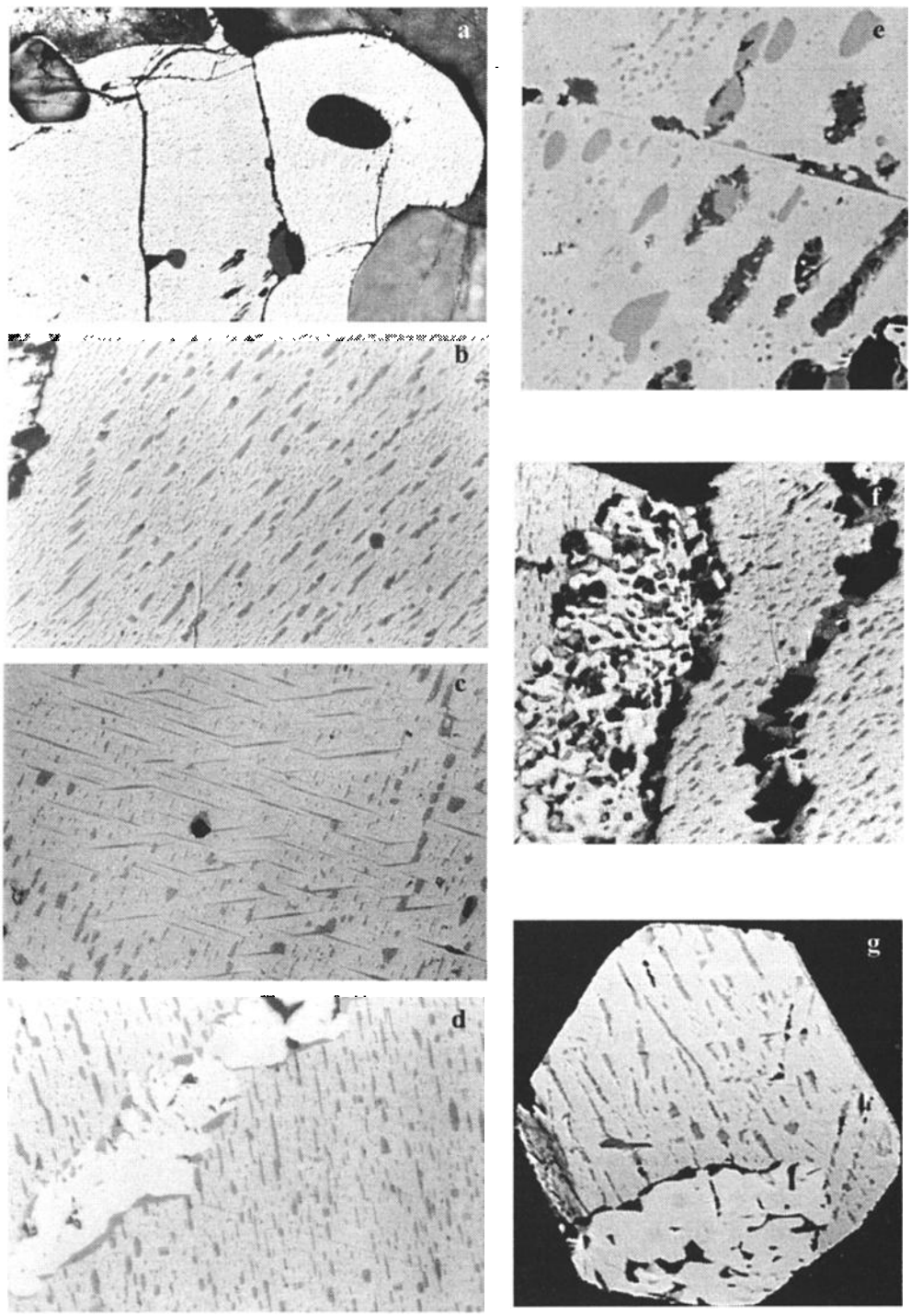

Figure 3. Photomicrographs of polished thin sections from the Russell Belt microcline gneiss. (a) Titanohematite grain with {0001} ilmenite and pyrophanite exsolution lamellae. Note lack of alteration at titanohematite grain boundaries. Field of view 330 μm. (b) Multiple generations of ilmenite lamellae (darker gray) in titanohematite grain. Black lamellae are spinel and corundum. Field of view 60 μm. (c) Very fine ilmenite and pyrophanite lamellae in titanohematite. Spinel exsolution (black) is commonly internal to ilmenite lamellae. Rutile needles are also common. Note titanohematite areas near rutile needles are usually free of ilmenite exsolution. Field of view 60 μm. (d) Very fine ilmenite lamellae in titanohematite. Note a hematite (pure white) zone rimmed by rutile (dark gray) and small amounts of spinel (black). These hematite + rutile areas are usually internal to the titanohematite grains. Field of view 300 μm. (e) Electron backscatter image of titanohematite host with spinel (black), large pyrophanite lamellae (darker gray), and smaller ilmenite lamellae. Note elaborate spinel + rutile rim around some pyrophanite lamellae. Field of view 60 μm. f) Titanohematite grain with ilmenite lamellae and an internal symplectite of hematite (white), rutile (gray), and spinel (black). Ilmenite, pyrophanite, and spinel exsolution border the symplectite and titanohematite host grain and also form a separate symplectite on the right. (g) Electron backscatter image of a composite titanohematite grain with ilmenite lamellae and adjacent magnetite grain. A rutile rim (black) is at the border between magnetite and the titanohematite. Discrete areas of rutile are internal to the magnetite. Field of view 60 μm All photomicrographs were made with a blue filter, in oil immersion, and under crossed polars.

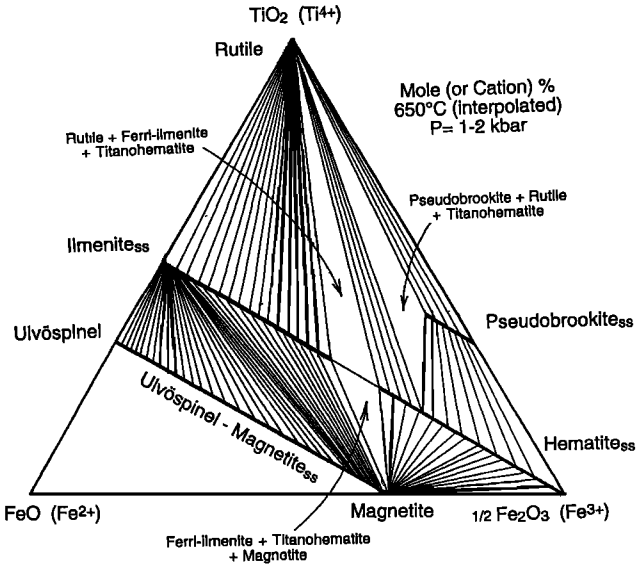

Figure 4. Approximate equilibrium phase diagram for the system FeO-TiO_2-$1/2Fe_2O_3$ (Fe^{2+}-Ti^{4+}-Fe^{3+}) at 650°C. Interpolated from Figure 8, 800°C and 600°C diagrams, of *Lindsley* [1991] but with width of the ilmenite-hematite two-phase field taken from *Burton* [1991]. This illustrates probable phase relations in the very oxidized part of the diagram close to the TiO_2-$1/2Fe_2O_3$ join. Of special interest is the three-phase field pseudobrookite-rutile-titanohematite which migrates toward the right with falling temperature until end-member pseubobrookite breaks down to rutile and end-member hematite at ~580°C. This illustrates how an assemblage titanohematite-titanian pseudobrookite at 650°C could break down at lower temperatures to less titanian hematite plus rutile-titanohematite pseudomorphs after pseudobrookite as suggested by textural features in Figure 3f.

Exsolution of pyrophanite ($MnTiO_3$), usually more blocky in shape and darker beige in color than the ilmenite, occurs in rows parallel to {0001}. The pyrophanite may be intergrown with, or rimmed by, spinel and/or rutile (Figures 3e and 3f). Spinel and corundum are present as exsolution products, usually within ilmenite lamellae though not restricted to them. Three sets of rutile needles or plates (Figure 3c) parallel to {2243} [*Ramdohr*, 1969] are common in the titanohematite grains (Figure 3d). On the basis of optical observations, rutile appears to have formed in a high-temperature reaction before ilmenite was "exsolved" from hematite. The rutile needles are usually confined to the centers of the titanohematite grains. Very small sulfide inclusions or exsolutions are in ilmenite lamellae, though not restricted to them. Locally, there are discrete symplectites and patches of Ti-poor hematite + rutile (Figure 3b) usually internal to the titanohematite grains (Figure 3d). The symplectites (Figure 3f) may have formed as a breakdown product of pseudobrookite (Figure 4) as these rocks cooled from peak metamorphic conditions of ~700-650°C to temperatures below 580°C, where pseudobrookite would be unstable [*Lindsley*, 1991]. At low temperature, below 400°C, ilmenite can break down to hematite + rutile by oxidation. This reaction is represented in some large first-generation ilmenite lamellae decomposed to hematite + rutile ± spinel. Though this decomposition was observed in some lamellae, there are also abundant pristine first-generation ilmenite lamellae. Discrete MD size grains of magnetite are rare. Figure 3g shows a magnetite adjacent to titanohematite. A rutile rim is present at the boundary, and internal to the magnetite there are discrete areas of rutile. This suggests that reaction of ilmenite + hematite to magnetite + rutile took place at a maximum temperature of 400°C [*Lindsley*, 1991]. Such magnetite-rutile assemblages are widespread elsewhere in greenschist-facies regional metamorphic rocks [*Rumble*, 1976]. Small rare magnetite inclusions which lack exsolution or oxidation-exsolution lamellae occur in a few titanohematite grains. Late goethite rims surround ~2% of the titanohematite grains. Despite the strong evidence in altered biotite and plagioclase, for significant post metamorphic hydrothermal alteration, many features of the oxide mineralogy appear to reflect the high-temperature part of the cooling from peak-metamorphic upper amphibolite- to granulite-facies regional metamorphism.

Hematite grains with multiple generations of ilmenite and rutile lamellae and hematite grains free of apparent exsolution were analyzed by microprobe in seven specimens. Calculated mineral formulas of representative analyses are listed in Table 1. The hematite grains without exsolution are nearly end-member hematite with compositions 98-100% Fe_2O_3. The remaining components, up to 2%, are composed of ilmenite ($FeTiO_3$), geikielite ($MgTiO_3$), and smaller amounts of pyrophanite ($MnTiO_3$) and $CaTiO_3$. Micron-size inclusions of muscovite throughout the hematite are common. The discrete grains of exsolution-free hematite may be secondary.

Traverses across titanohematite host grains with ilmenite exsolution and rutile needles show that the hematite-rich areas range from 72 to 97% hematite component. The most hematite-rich compositions were analyzed near rutile needles. These areas are typically composed of $hematite_{97-98}$, with up to 2% ilmenite component ($FeTiO_3$), and 1% of $MnTiO_3$, $CaTiO_3$ and $MgTiO_3$ combined. The most hematite-poor composition, $hematite_{72}$, contains 27% ilmenite component in solid solution with $MnTiO_3$, $CaTiO_3$ and $MgTiO_3$ combined to contribute 1%. "Clean" spot analyses of the host titanohematite grains, in areas where "exsolution" was not observed with the microprobe at a magnification of 5000x, had typical compositions of $hematite_{83}$. It is quite possible that there may be ultra-fine exsolution within the titanohematite grains not observable at this scale. If these are "true" analyses, then they would represent a metastable hematite composition. It is quite possible that diffusion became so sluggish with cooling to temperatures below 450°C that further exsolution could not occur, resulting in these metastable compositions.

The ilmenite lamellae have a range in composition from $ilmenite_{97-70}$, with 6-14% pyrophanite ($MnTiO_3$), 1-13%, averaging 5% hematite, up to 2% $CaTiO_3$ and $MgTiO_3$, and up to 1% eskolaite (Cr_2O_3) and 1% karelianite (V_2O_3) component. Ilmenite lamellae are

Table 1. Representative Formulae from Hematite, Titanohematite, Ilmenite and Pyrophanite Analyses in the Russell Gneisses Based on 2 Cations and 3 Oxygens.

Mineral Phase	Octahedral layer 1	Octahedral layer 2
	RS1-5	
Hematite exsolution free	Octahedral layer	Octahedral layer
$Hematite_{99\ 5}$	$Fe^{3+}_{.995}Fe^{2+}_{005}$	$Fe^{3+}_{995}Fe^{2+}_{.005}$
$Hematite_{92}$	$Fe^{3+}_{92}Al^{3+}_{04}Fe^{2+}_{02}(Mn, Mg,Cr)_{02}$	$Fe^{3+}_{92}Al^{3+}_{04}Fe^{2+}_{02}(Mn, Mg, Cr)_{02}$
Titanohematite	Octahedral layer	Octahedral layer
$Hematite_{81}$	$Fe^{3+}_{81}Fe^{2+}_{09}Mn^{2+}_{01}Ti^{4+}_{09}$	$Fe^{3+}_{81}Fe^{2+}_{09}Mn^{2+}_{01}Ti^{4+}_{09}$
$Hematite_{78}$	$Fe^{3+}_{78}Fe^{2+}_{10}Mn^{2+}_{01}Ti^{4+}_{.11}$	$Fe^{3+}_{78}Fe^{2+}_{.10}Mn^{2+}_{01}Ti^{4+}_{11}$
$Hematite_{72}$	$Fe^{3+}_{72}Fe^{2+}_{13}Mn^{2+}_{01}Ti^{4+}_{14}$	$Fe^{3+}_{72}Fe^{2+}_{.13}Mn^{2+}_{01}Ti^{4+}_{.14}$
Ilmenite lamellae	Fe-Octahedral layer	Ti-Octahedral layer
$Ilmenite_{96}$	$Fe^{2+}_{83}Mn^{2+}_{.12}Fe^{3+}_{.04}Mg^{2+}_{.01}$	$Ti^{4+}_{96}Fe^{3+}_{.04}$
$Ilmenite_{95}$	$Fe^{2+}_{82}Mn^{2+}_{.12}Fe^{3+}_{.05}Mg^{2+}_{.01}$	$Ti^{4+}_{95}Fe^{3+}_{05}$
	RS1-6	
Hematite exsolution free	Octahedral layer	Octahedral layer
$Hematite_{99}$	$Fe^{3+}_{.99}Al^{3+}_{01}$	$Fe^{3+}_{.99}Al^{3+}_{.01}$
$Hematite_{98}$	$Fe^{3+}_{98}Al^{3+}_{.01}Si^{4+}_{.01}$	$Fe^{3+}_{98}Al^{3+}_{.01}Si^{4+}_{01}$
Titanohematite	Octahedral layer	Octahedral layer
$Hematite_{90}$	$Fe^{3+}_{90}Fe^{2+}_{05}\ Ti^{4+}_{05}$	$Fe^{3+}_{90}Fe^{2+}_{05}\ Ti^{4+}_{.05}$
$Hematite_{85}$	$Fe^{3+}_{.85}Fe^{2+}_{07}\ Ti^{4+}_{.08}$	$Fe^{3+}_{.85}Fe^{2+}_{07}\ Ti^{4+}_{.08}$
$Hematite_{83}$	$Fe^{3+}_{.83}Fe^{2+}_{085}Ti^{4+}_{.085}$	$Fe^{3+}_{.83}Fe^{2+}_{085}Ti^{4+}_{.085}$
$Hematite_{82}$	$Fe^{3+}_{82}Fe^{2+}_{.075}Mn^{2+}_{.015}Ti^{4+}_{09}$	$Fe^{3+}_{.82}Fe^{2+}_{.075}Mn^{2+}_{.015}Ti^{4+}_{09}$
$Hematite_{80}$	$Fe^{3+}_{.80}Fe^{2+}_{085}Mn^{2+}_{.015}Ti^{4+}_{10}$	$Fe^{3+}_{.80}Fe^{2+}_{085}Mn^{2+}_{.015}Ti^{4+}_{.10}$
Ilmenite lamellae	Fe-Octahedral layer	Ti-Octahedral layer
$Ilmenite_{98}$	$Fe^{2+}_{91}Mn^{2+}_{08}Fe^{3+}_{.01}$	$Ti^{4+}_{.98}Fe^{3+}_{.02}$
$Ilmenite_{97}$	$Fe^{2+}_{.88}Mn^{2+}_{09}Fe^{3+}_{03}$	$Ti^{4+}_{.97}Fe^{3+}_{03}$
$Ilmenite_{96}$	$Fe^{2+}_{84}Mn^{2+}_{12}Fe^{3+}_{04}$	$Ti^{4+}_{96}Fe^{3+}_{04}$
$Ilmenite_{95}$	$Fe^{2+}_{88}Mn^{2+}_{07}Fe^{3+}_{04}Mg^{2+}_{01}$	$Ti^{4+}_{95}Fe^{3+}_{05}$
	RS2-2	
Hematite exsolution free	Octahedral layer	Octahedral layer
$Hematite_{99.6}$	$Fe^{3+}_{.996}Mn^{2+}_{.004}$	$Fe^{3+}_{996}Mn^{2+}_{.004}$
$Hematite_{98}$	$Fe^{3+}_{.98}\ Fe^{2+}_{.01}Ti^{4+}_{01}$	$Fe^{3+}_{.98}\ Fe^{2+}_{.01}Ti^{4+}_{01}$
$Hematite_{96}$	$Fe^{3+}_{96}\ Fe^{2+}_{.01}Al^{3+}_{01}Mg^{2+}_{.01}Ti^{4+}_{01}$	$Fe^{3+}_{.96}\ Fe^{2+}_{.01}Al^{3+}_{.01}Mg^{2+}_{01}Ti^{4+}_{01}$
Titanohematite	Octahedral layer	Octahedral layer
$Hematite_{83}$	$Fe^{3+}_{83}Fe^{2+}_{.07}Mn^{2+}_{.01}Ti^{4+}_{.09}$	$Fe^{3+}_{.83}Fe^{2+}_{07}Mn^{2+}_{.01}Ti^{4+}_{.09}$
$Hematite_{82}$	$Fe^{3+}_{.82}Fe^{2+}_{09}Ti^{4+}_{09}$	$Fe^{3+}_{.82}Fe^{2+}_{09}Ti^{4+}_{.09}$
$Hematite_{78}$	$Fe^{3+}_{.78}Fe^{2+}_{.11}Ti^{4+}_{11}$	$Fe^{3+}_{78}Fe^{2+}_{.11}Ti^{4+}_{11}$
Ilmenite lamellae	Fe-Octahedral layer	Ti-Octahedral layer
$Ilmenite_{96}$	$Fe^{2+}_{.83}Mn^{2+}_{12}Mg^{2+}_{01}Fe^{3+}_{.04}$	$Ti^{4+}_{.96}Fe^{3+}_{.04}$
$Ilmenite_{95}$	$Fe^{2+}_{.80}Mn^{2+}_{14}Mg^{2+}_{01}Fe^{3+}_{.05}$	$Ti^{4+}_{.95}Fe^{3+}_{.05}$
	RS 6-1	
Hematite exsolution free	Octahedral layer	Octahedral layer
$Hematite_{100}$	$Fe^{3+}_{1.0}$	$Fe^{3+}_{1.0}$
Titanohematite	Octahedral layer	Octahedral layer
$Hematite_{88}$	$Fe^{3+}_{88}Fe^{2+}_{055}Ti^{4+}_{055}$	$Fe^{3+}_{88}Fe^{2+}_{.055}Ti^{4+}_{055}$
$Hematite_{84}$	$Fe^{3+}_{.84}Fe^{2+}_{.08}Ti^{4+}_{.08}$	$Fe^{3+}_{.84}Fe^{2+}_{.08}Ti^{4+}_{08}$
$Hematite_{84}$	$Fe^{3+}_{.84}Fe^{2+}_{.08}Ti^{4+}_{08}$	$Fe^{3+}_{84}Fe^{2+}_{.08}Ti^{4+}_{08}$
$Hematite_{82}$	$Fe^{3+}_{.82}Fe^{2+}_{09}Ti^{4+}_{.09}$	$Fe^{3+}_{.82}Fe^{2+}_{.09}Ti^{4+}_{.09}$
$Hematite_{80}$	$Fe^{3+}_{80}Fe^{2+}_{10}Ti^{4+}_{095}V^{3+}_{005}$	$Fe^{3+}_{80}Fe^{2+}_{10}Ti^{4+}_{095}V^{3+}_{.005}$
$Hematite_{77}$	$Fe^{3+}_{.77}Fe^{2+}_{.22}Ti^{4+}_{23}Mn^{2+}_{.01}$	$Fe^{3+}_{.77}Fe^{2+}_{22}Ti^{4+}_{23}Mn^{2+}_{.01}$
Ilmenite lamellae	Fe-Octahedral layer	Ti-Octahedral layer
$Ilmenite_{97}$	$Fe^{2+}_{87}Mn^{2+}_{.10}Fe^{3+}_{.03}$	$Ti^{4+}_{97}Fe^{3+}_{03}$
$Ilmenite_{96}$	$Fe^{2+}_{86}Mn^{2+}_{10}Fe^{3+}_{.04}$	$Ti^{4+}_{.96}Fe^{3+}_{04}$
$Ilmenite_{90}$	$Fe^{2+}_{.81}Mn^{2+}_{08}Ca^{2+}_{01}Fe^{3+}_{10}$	$Ti^{4+}_{90}Fe^{3+}_{.10}$
$Ilmenite_{86}$	$Fe^{2+}_{.79}Mn^{2+}_{08}Fe^{3+}_{.13}$	$Ti^{4+}_{86}Fe^{3+}_{13}V^{3+}_{.01}$

Table 1. (continued)

Mineral Phase	Octahedral layer 1	Octahedral layer 2
	RS6-2	
Hematite exsolution free	Octahedral layer	Octahedral layer
$Hematite_{100}$	$Fe^{3+}_{1.0}$	$Fe^{3+}_{1.0}$
$Hematite_{98}$	$Fe^{3+}_{.98}Fe^{2+}_{.01}Ti^{4+}_{.01}$	$Fe^{3+}_{.98}Fe^{2+}_{.01}Ti^{4+}_{.01}$
Titanohematite	Octahedral layer	Octahedral layer
$Hematite_{86}$	$Fe^{3+}_{.86}Fe^{2+}_{.07}Ti^{4+}_{.07}$	$Fe^{3+}_{.86}Fe^{2+}_{.07}Ti^{4+}_{.07}$
$Hematite_{85}$	$Fe^{3+}_{.85}Fe^{2+}_{.075}Ti^{4+}_{.075}$	$Fe^{3+}_{.85}Fe^{2+}_{.075}Ti^{4+}_{.075}$
$Hematite_{83}$	$Fe^{3+}_{.83}Fe^{2+}_{.085}Ti^{4+}_{.085}$	$Fe^{3+}_{.83}Fe^{2+}_{.085}Ti^{4+}_{.085}$
$Hematite_{76}$	$Fe^{3+}_{.76}Fe^{2+}_{.12}Ti^{4+}_{.12}$	$Fe^{3+}_{.76}Fe^{2+}_{.12}Ti^{4+}_{.12}$
Ilmenite lamellae	Fe-Octahedral layer	Ti-Octahedral layer
$Ilmenite_{99}$	$Fe^{2+}_{.19}Mn^{2+}_{.80}Fe^{3+}_{.01}$	$Ti^{4+}_{.99}Fe^{3+}_{.005}V^{3+}_{.005}$
$Ilmenite_{98}$	$Fe^{2+}_{.56}Mn^{2+}_{.41}Fe^{3+}_{.03}$	$Ti^{4+}_{.98}Fe^{3+}_{.02}$
$Ilmenite_{97}$	$Fe^{2+}_{.25}Mn^{2+}_{.71}Fe^{3+}_{.03}Mg^{2+}_{.01}$	$Ti^{4+}_{.97}Fe^{3+}_{.03}$
$Ilmenite_{96}$	$Fe^{2+}_{.86}Mn^{2+}_{.09}Fe^{3+}_{.04}Mg^{2+}_{.01}$	$Ti^{4+}_{.96}Fe^{3+}_{.04}$
$Ilmenite_{95}$	$Fe^{2+}_{.49}Mn^{2+}_{.46}Fe^{3+}_{.05}$	$Ti^{4+}_{.95}Fe^{3+}_{.05}$
	RS34-6b	
Hematite exsolution free	Octahedral layer	Octahedral layer
$Hematite_{100}$	$Fe^{3+}_{1.0}$	$Fe^{3+}_{1.0}$
$Hematite_{98}$	$Fe^{3+}_{.98}Fe^{2+}_{.01}Ti^{4+}_{.01}$	$Fe^{3+}_{.98}Fe^{2+}_{.01}Ti^{4+}_{.01}$
Titanohematite	Octahedral layer	Octahedral layer
$Hematite_{85}$	$Fe^{3+}_{.84}Fe^{2+}_{.075}Ti^{4+}_{.075}$	$Fe^{3+}_{.84}Fe^{2+}_{.075}Ti^{4+}_{.075}$
$Hematite_{84}$	$Fe^{3+}_{.84}Fe^{2+}_{.08}Ti^{4+}_{.08}$	$Fe^{3+}_{.84}Fe^{2+}_{.08}Ti^{4+}_{.08}$
$Hematite_{83}$	$Fe^{3+}_{.83}Fe^{2+}_{.17}$	$Fe^{3+}_{.83}Fe^{2+}_{.17}$
$Hematite_{82}$	$Fe^{3+}_{.82}Fe^{2+}_{.09}Ti^{4+}_{.09}$	$Fe^{3+}_{.82}Fe^{2+}_{.09}Ti^{4+}_{.09}$
$Hematite_{81}$	$Fe^{3+}_{.81}Fe^{2+}_{.095}Ti^{4+}_{.095}$	$Fe^{3+}_{.81}Fe^{2+}_{.095}Ti^{4+}_{.095}$
Ilmenite lamellae	Fe-Octahedral layer	Ti-Octahedral layer
$Ilmenite_{98}$	$Fe^{2+}_{.92}Mn^{2+}_{.06}Mg^{2+}_{.01}Fe^{3+}_{.01}$	$Ti^{4+}_{.98}Fe^{3+}_{.02}$
$Ilmenite_{98}$	$Fe^{2+}_{.90}Mn^{2+}_{.07}Fe^{3+}_{.03}$	$Ti^{4+}_{.98}Fe^{3+}_{.02}$
$Ilmenite_{96}$	$Fe^{2+}_{.89}Mn^{2+}_{.07}Mg^{2+}_{.01}Fe^{3+}_{.03}$	$Ti^{4+}_{.96}Fe^{3+}_{.04}$
$Ilmenite_{95}$	$Fe^{2+}_{.89}Mn^{2+}_{.06}Mg^{2+}_{.01}Fe^{3+}_{.04}$	$Ti^{4+}_{.95}Fe^{3+}_{.05}$
	RS34-7	
Hematite exsolution free	Octahedral layer	Octahedral layer
$Hematite_{100}$	$Fe^{3+}_{1.0}$	$Fe^{3+}_{1.0}$
$Hematite_{98}$	$Fe^{3+}_{.98}Al^{3+}_{.01}Mn^{3+}_{.01}$	$Fe^{3+}_{.98}Al^{3+}_{.01}Mn^{3+}_{.01}$
Titanohematite	Octahedral layer	Octahedral layer
$Hematite_{84}$	$Fe^{3+}_{.84}Fe^{2+}_{.08}Ti^{4+}_{.08}$	$Fe^{3+}_{.84}Fe^{2+}_{.08}Ti^{4+}_{.08}$
$Hematite_{83}$	$Fe^{3+}_{.83}Fe^{2+}_{.08}Ti^{4+}_{.09}$	$Fe^{3+}_{.83}Fe^{2+}_{.08}Ti^{4+}_{.09}$
$Hematite_{82}$	$Fe^{3+}_{.83}Fe^{2+}_{.09}Ti^{4+}_{.09}$	$Fe^{3+}_{.83}Fe^{2+}_{.09}Ti^{4+}_{.09}$
$Hematite_{72}$	$Fe^{3+}_{.72}Fe^{2+}_{.27}Mn^{2+}_{.01}$	$Fe^{3+}_{.72}Fe^{2+}_{.27}Mn^{2+}_{.01}$
Ilmenite lamellae	Fe-Octahedral layer	Ti-Octahedral layer
$Ilmenite_{99}$	$Fe^{2+}_{.91}Mn^{2+}_{.07}Mg^{2+}_{.01}Fe^{2+}_{.01}$	$Ti^{4+}_{.99}Fe^{3+}_{.01}$
$Ilmenite_{98}$	$Fe^{2+}_{.83}Mn^{2+}_{.15}Mg^{2+}_{.01}Ca^{2+}_{.01}Fe^{3+}_{.01}$	$Ti^{4+}_{.98}Fe^{3+}_{.02}$
$Ilmenite_{97}$	$Fe^{2+}_{.87}Mn^{2+}_{.10}Mg^{2+}_{.01}Fe^{3+}_{.02}$	$Ti^{4+}_{.97}Fe^{3+}_{.03}$
$Ilmenite_{96}$	$Fe^{2+}_{.89}Mn^{2+}_{.06}Mg^{2+}_{.01}Fe^{3+}_{.04}$	$Ti^{4+}_{.96}Fe^{3+}_{.03}V^{3+}_{.01}$
$Ilmenite_{95}$	$Fe^{2+}_{.87}Mn^{2+}_{.08}Mg^{2+}_{.01}Fe^{3+}_{.04}$	$Ti^{4+}_{.95}Fe^{3+}_{.04}V^{3+}_{.01}$

In all formulae the atoms are distributed between two layers. In disordered $R\bar{3}c$ hematite and titanohematite the distribution is even between the layers. Examination of a single layer allows direct reading of percent hematite (from Fe^{3+}), ilmenite (from Ti^{4+}). In ordered $R\bar{3}$ ilmenite, all Ti is distributed to the Ti-octahedral layer, and all Fe^{2+}, Mn^{2+}, Mg^{2+} are distributed to the Fe-octahedral layer. Percent hematite is read directly from the Fe^{3+} in the Ti-octahedral layer, % ilmenite, pyrophanite, geikielite, etc. are read directly from the Fe^{2+}, Mn^{2+}, and Mg^{2+} in the Fe-octahedral layer.

closer to end-member compositions than the titanohematite host, with a typical composition of ilmenite$_{96}$, implying an asymmetry toward ilmenite of the hematite-ilmenite two-phase field. This is expected due to the greater solubility of ilmenite in hematite (see *Burton* [1991] for details). Abundant pyrophanite (Mn, $FeTiO_3$) lamellae in hematite may have up to 80% $MnTiO_3$ component. Locally, internal to titanohematite are discrete patches of hematite + rutile that are nearly end-member with compositions of hematite$_{99}$ + rutile$_{100}$ (Figure 3d). Ilmenorutile (Ti, Nb, $Fe^{3+}O_3$) is found in the titanohematite and is associated with spinel, rutile and pyrophanite as shown in Figure 3e.

Rare magnetite as inclusions or discrete grains, was found in a few samples. An electron backscatter image (Figure 3g) shows coexisting titanohematite, magnetite, and rutile. Chemical data showed magnetite to be nearly end-member with 99% magnetite component combined with minor amounts of TiO_2, Al_2O_3, and MnO.

5. Paleomagnetism and Rock Magnetism

5.1. Sampling

The six sites discussed here are from the microcline-sillimanite gneiss (gms unit) in the Russell area (Figure 1), a subset of a larger Adirondack paleomagnetic project. Thirty-six cores were drilled with a gasoline-powered drill and oriented using a brass orienting sleeve with magnetic and solar compasses or were drilled from oriented blocks in the laboratory.

5.2. Laboratory Procedures

A significant part of the natural remanent magnetization (NRM) may be carried by SD or pseudo-single-domain (PSD) size grains. Due to the small domain size for magnetite, it is important to combine optical and compositional data with rock magnetic properties to help constrain the magnetic mineralogy. The NRM measurements were made on a 2G SQUID magnetometer at the University of Massachusetts, Amherst. After NRM measurements, progressive alternating and thermal demagnetization procedures were used to isolate the characteristic or primary components. Alternating field (AF) demagnetization was performed up to 100 mT on selected samples and thermal demagnetization up to 680°C on most samples using a Molspin AF demagnetizer and an ASC thermal demagnetizer, respectively. Magnetic susceptibility values were measured on a Sapphire Instruments susceptibility bridge. Hysteresis measurements, both at room temperature and with elevated temperature, in a field of up to 2T (micromagnetometer or vibrating sample magnetometer, Princeton Applied Research), and low-temperature remanence measurements on a Quantum Design (MPMS2) Squid magnetometer were made at the Institute for Rock Magnetism, University of Minnesota.

5.3. Rock Magnetic Properties

There is a large range in NRM intensities (Table 2) from 10^{-3} to 10^{1} A/m, as would be expected from a layered rock unit with considerable original variation in bulk chemistry. When these rock layers were metamorphosed to granulite facies, various oxides were produced in varied abundances in the different layers, dependent on the original bulk chemistry. The average NRM intensity for the gms unit is 3.6 A/m. NRM directions (Figure 5) are generally west and negative (up). Susceptibility varies over 3 orders of magnitude from $1x10^{-4}$ to $1x10^{-2}$ SI units, with a mean of $2.3x10^{-4}$ and a median of $4.2x10^{-4}$. Though on average the gms unit has very low susceptibility values, there is a wide susceptibility range, which reflects the local compositional variations within the unit.

Progressive demagnetization reveals that most samples have a very high magnetic stability and a single-component magnetization. AF demagnetization to 100 mT had little effect on remanence, with only a small decay in the original NRM and a slight change in direction (Figure 6). Thermomagnetic runs show the NRM is stable with little loss until high temperatures and shows only small directional changes. The monitoring of susceptibility after each heating step suggests no alteration of the magnetic minerals with temperature. Samples either show a slight loss in remanence below 580°C or show no loss until 600°C (Figure 6). Samples which do have a remanence loss below 580°C characteristically have very little decay until 550°C, then usually between 2 and 10% loss, or very rarely up to a 30% loss, between 550°C and 580°C (Figure 6b). Above 600°C, all samples have steady and rapid decrease in magnetization to 670 or 680°C. Samples that do not show a loss in magnetization until 600°C have an average loss of ~5% at 600°C followed by a steady decrease in magnetization to 670-680°C (Figure 6). In general, samples retain 90% or more of the original NRM component to 600°C and have a median destructive thermal temperature of ~640°C, clearly indicating a large hematite contribution to the NRM.

5.4. Saturation Isothermal Remanent Magnetization (SIRM)

Russell Gneiss samples contain a mixed magnetic mineralogy of titanohematite, hematite, and ferrianilmenite ± magnetite. Samples that contain even a small amount of magnetite should show a significant acquisition at lower fields than samples with only hematite + titanohematite assemblages. All samples have MD to SD titanohematite grains. Given the broad grain size range for SD behavior in hematite, from ~0.03 to 15 μm [*Dunlop and Özdemir*, 1997] most samples should show a large SD contribution. Grains up to a few hundred microns in size contain only a few domains and should exhibit PSD behavior. Millimeter size grains may contribute a "softer MD" component, while others will have an "SD" component caused by the extensive fine-scale microtextures within the large grains. Many of the second or third generation hematite lamellae may be superparamagnetic because they are smaller than ~0.03μm [*Banerjee*, 1971].

The Russell samples show a variety of responses to applied magnetic fields (Figure 7). Samples with the rare discrete MD magnetites (RS6-1) acquire 60% of their SIRM by 0.1 T and nearly 70% by 0.15 T, though full saturation is not obtained until above 0.5 T. The

Table 2. Magnetic Properties of Oriented Cores from Microcline Granite Gneiss, Russell Belt

Sample	SUSC (10^{-4})	NRM	*Q*	*Hc*	*Hcr/Hc*	*Ms*	*Mrs/Ms*	*I*	*D*
RS1-1	1.94	2.882	323	**	**	**	**	-57.2	206.6
RS1-2	2.40	3.311	300	**	**	**	**	-57.4	240.5
RS1-3	2.38	3.763	344	**	**	**	**	-53.9	221.4
RS1-4	3.12	3.995	278	135	1.28	13.6	0.555	-56.2	235.4
RS1-5	9.52	7.949	182	148	1.27	24.4	0.475	-69.1	218.4
RS1-6	5.54	8.958	352	130	1.18	11.3	0.491	-67.6	233.1
RS1-7	1.70	1.218	156	181	0.99	30.2	0.796	-70.4	112.6
RS2-1	1.25	0.019	3.3	**	**	**	**	-47.3	243.7
RS2-3	1.83	0.025	3.1	**	**	**	**	-38.2	193.1
RS2-4	4.13	0.107	5.6	**	**	**	**	-66.1	248.4
RS2-5	5.61	0.534	21	**	**	**	**	-51.2	274.8
RS2-6	1.89	0.019	2.2	**	**	**	**	-55.8	260.9
RS3-A	16.60	0.029	0.4	44	3.15	83.9	0.257	-33.8	269.8
RS3-B	19.90	0.087	1	18	7.03	106	0.135	-44.7	337.2
RS4-A	0.88	0.003	0.7	266	2.01	1.77	0.739	-39.3	285.3
RS6-1-1	144.00	2.882	4.4	123	2.16	21.8	0.311	-62.9	286.7
RS6-1-2	269.00	2.252	1.8	129	2.41	18.3	0.372	-71.1	293.1
RS6-1-3	129.00	3.841	6.5	**	**	**	**	-64.2	290.6
RS6-2-1	3.72	0.145	8.5	**	**	**	**	-43.1	285.7
RS6-2-2	4.80	0.832	38	120	2.41	14.8	0.325	-29.5	273.7
RS6-2-3	4.62	0.058	2.7	**	**	**	**	-37	315.1
RS6-2-4	7.86	1.431	40	**	**	**	**	-48.7	300.5
RS6-2-5	3.39	0.622	39	**	**	**	**	-67.1	271.7
RS6-2-6	7.11	0.561	17	15	18.34	118	0.131	-53.2	299.6
RS6-2-7	5.50	0.888	35	15	8.87	15.1	0.279	-36.2	297.6
AD34-1	4.18	8.143	424	**	**	**	**	-54.6	245.4
AD34-2	1.84	7.775	918	**	**	**	**	-22.4	258.7
AD34-3	3.69	7.511	443	**	**	**	**	-62.5	247.2
AD34-4A	13.80	7.736	122	**	**	**	**	-56.1	266.8
AD34-4B	69.70	7.096	22	**	**	**	**	-63.3	268.3
AD34-5	3.27	8.453	562	**	**	**	**	-61.5	263.4
AD34-6A	4.86	5.931	266	**	**	**	**	-60.7	275.3
AD34-6B	2.99	8.231	598	**	**	**	**	-51.1	274.3
AD34-7	99.10	7.579	17	**	**	**	**	-54.4	277.9
AD34-8A	3.79	7.749	444	**	**	**	**	-54.4	254.7
AD34-8B	12.50	6.946	121	**	**	**	**	-58.9	257.2
Mean	22.6	3.598	170	**	**	**	**	-58.2	266.4
Mean NRM vector	22.6	3.462	33	**	**	*	**	-59.0	257.9

SUSC, susceptibility in SI units; NRM, intensity of sample before demagnetization, in A/m; *Q*, Koenigsberger ratio; *Hc*, coercivity in mT; *Hcr/Hc*, ratio of remanence coercivity to coercivity; *Ms*, saturation magnetization in mAm^2/kg; *Mrs/Ms*, ratio of remanent magnetization to saturation magnetization; *I* and *D*, inclination and declination of natural remanent magnetization, in degrees. Mean is paleomagnetic mean direction calculated by assigning unit weight to samples directions. Mean NRM vector is sum of NRM vectors/number of vector.

NRM/SIRM ratio indicates this sample was 5% saturated in its natural state. Magnetite and MD hematite contribute to the low-field acquisition, with SD titanohematite contributing to the high-field portion. Samples from site RS6-2 show only a limited saturation of ~ 25% by 0.15 T, and by 0.5 T the curves are starting to shoulder, indicating that they are close to saturation. The NRM/SIRM ratios are from 1 to 2%.

Samples RS1-4 and RS1-6 have acquisition curves markedly different from those discussed above and significantly displaced from the origin at the onset of the experiment. Upon applying a field, a decrease in saturation is initially observed up to 0.1 T. This behavior is attributed to the geometry of the applied field relative to the remanent vector. Above 0.1 to 0.15 T, 25-40% saturation is achieved, followed by a continued increase in saturation to 0.7 T. Above 0.7 T, acquisition starts to level off, and by 1.3 T the samples, though not fully saturated, are nearly so. The NRM/SIRM ratios indicate that these samples are up to 25% saturated in the NRM state. Though most of the Russell samples are dominated by titanohematite grains that are larger than the upper limit for SD hematite, the abundant fine-scale microtextures in the titanohematite grains are likely to create regions with SD behavior, requiring higher applied fields to saturate than are needed for the MD hematites. In general, the acquisition behavior of these samples indicates a mixture of a high-coercivity material, such as a SD hematite, combined with a lower-coercivity material, such as MD hematite. Clearly, more experimental work needs to be done to fully understand the partially saturated state of these samples.

5.5. Hysteresis Properties

To understand further the magnetic phases, room temperature hysteresis loops were measured on representative samples. In addition, hysteresis properties were measured on a selected group of samples with temperature, starting at room temperature up to 700°C in 25°C intervals.

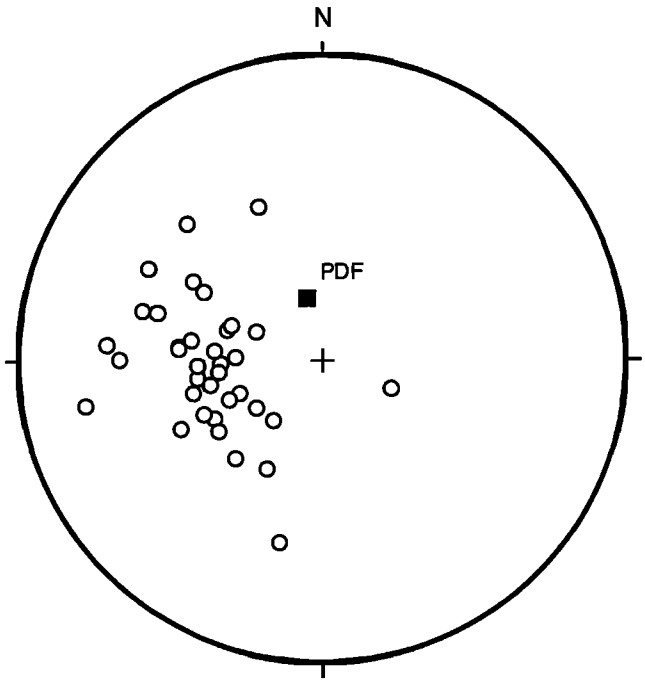

Figure 5. Natural remanent magnetization (NRM) directions of individual samples from the Russell Belt plotted on an equal area diagram. Open symbols indicate upward (negative) inclinations. PDF indicates the present day magnetic field direction for the Adirondack region.

Room temperature hysteresis loops display several types of behavior as a function of the mineralogy. Some samples show a restricted or "wasp-waisted" hysteresis loop (Figure 8a). A typical wasp-waisted sample has a coercive force of 123 mT, a saturation magnetization (Ms) of 21.8 mAm^2/kg and a saturation remanence (*Mrs*) of 6.79 mAm^2/kg. On average these samples have a ratio of coercivity of remanence to saturation coercivity (*Hcr/Hc*) of 2, though a few are higher. The average *Mrs/Ms* value is 0.25 with a maximum of 0.35 (Figure 9). We interpret these samples as having a significant SD-MD titanohematite component combined with a small amount of PSD or MD magnetite.

In contrast, other samples show a lozenge or hummingbird shape (Figures 8b, c). For this group the maximum coercive force measured is 266 mT, significantly higher than samples with the constricted loop. The Ms values are also higher, with a maximum value of Ms = 30.2 mAm^2/kg and a corresponding *Mrs* of = 24 mAm^2/kg. These samples have very high *Mrs/Ms* ratios, on average 0.5, with a maximum of 0.8, and *Hcr/Hc* values averaging 1.2 (Figure 9). The wasp-waisted and the hummingbird shape hysteresis curves are dominated by the titanohematite-hematite components. Both show relatively high magnetic saturation values, considering that the modal hematite content in the titanohematite is ~ 70%, and modal titanohematite in the rock is only 2-3%.

Elevated temperature hysteresis loops were measured on a subset of selected samples to increase our understanding of how these magnetic properties may vary with temperature and with depth in the Earth (Figure 10). All samples show a decrease in loop parameters at higher temperatures. Two characteristic loop shapes were found and are consistent with the two types discussed above. Hysteresis loops on samples with wasp-waisted behavior (Figure 10) clearly indicate that at least three components, or phases, are contributing to the magnetization. These samples retained the same shape and size hysteresis loop until 500°C. Between 500°C and 575°C the characteristic wasp-waisted shape is still evident but less constricted. By 600°C the constricted waist is no longer apparent, and the loop changes to a lozenge-shape. From 600°C to 675°C the hysteresis loop retains this shape but decreases in size. We interpret this behavior to reflect three different mineral phases, titanohematite and hematite as SD to MD size grains, coupled with PSD or MD magnetite. Magnetite would contribute a lower coercivity component up to 580°C. A titanium content of 10% in a SD or MD titanohematite would also lose its magnetization at lower temperatures than a pure hematite. The titanohematite host grains, many larger than 1 mm, may contribute a lower-coercivity component along with the magnetite, whereas the Ti-poorer titanohematite-hematite would continue to contribute a higher coercivity component with increasing temperature until 675°C. The gradient in the amount of remanence measured between 600°C and 675°C may well reflect compositional variation of the host titanohematite and exsolution lamellae, with higher temperatures reflecting the purer hematite.

In contrast, samples with a hummingbird shape at room temperature retain this shape until ~675°C. The overall behavior of these samples with increasing temperature is that the hysteresis loop retains the same shape but decreases in magnitude. We interpret this behavior as reflecting that (1) in the high-coercivity titanohematite-hematite, there is a range of grain sizes from SD to MD, with SD size dominating the loop, and (2) the change in size of the hysteresis loop with increasing temperature reflects the compositional variation in the titanohematite grains or lamellae. The titanium-richer hematite would lose its magnetization at lower temperatures. In both types of samples, *Mrs/Mr* ratios increase with increasing temperature. This is expected because the smaller SD hematite lamellae would be nearer to an end-member hematite composition.

5.6. Curie Temperatures

Thermomagnetic curves were obtained by running ~150 mg samples on a horizontal Curie balance with a magnetic induction of 0.8 T. Saturation magnetization (*Js*) was measured as a function of temperature (*T*) from 30°C to 700°C. The samples produced concave downward *Js-T* curves, with two of them reversible. Multiple Curie temperatures were determined from each of the *Js* versus *T* curves. Sample RS6-1, a magnetite-bearing sample, had a loss in magnetization between 550° C and 580°C followed by smaller decays at 630°C and 670°C. Sample RS1-7 had no observable magnetite and showed distinct losses in magnetization at 600°C and 630°C, followed by a very small decay at 670°C. Samples with Curie temperatures below 580°C can be attributed to near end-member magnetite and/or a Ti-richer titanohematite. Curie temperatures above 580°C,

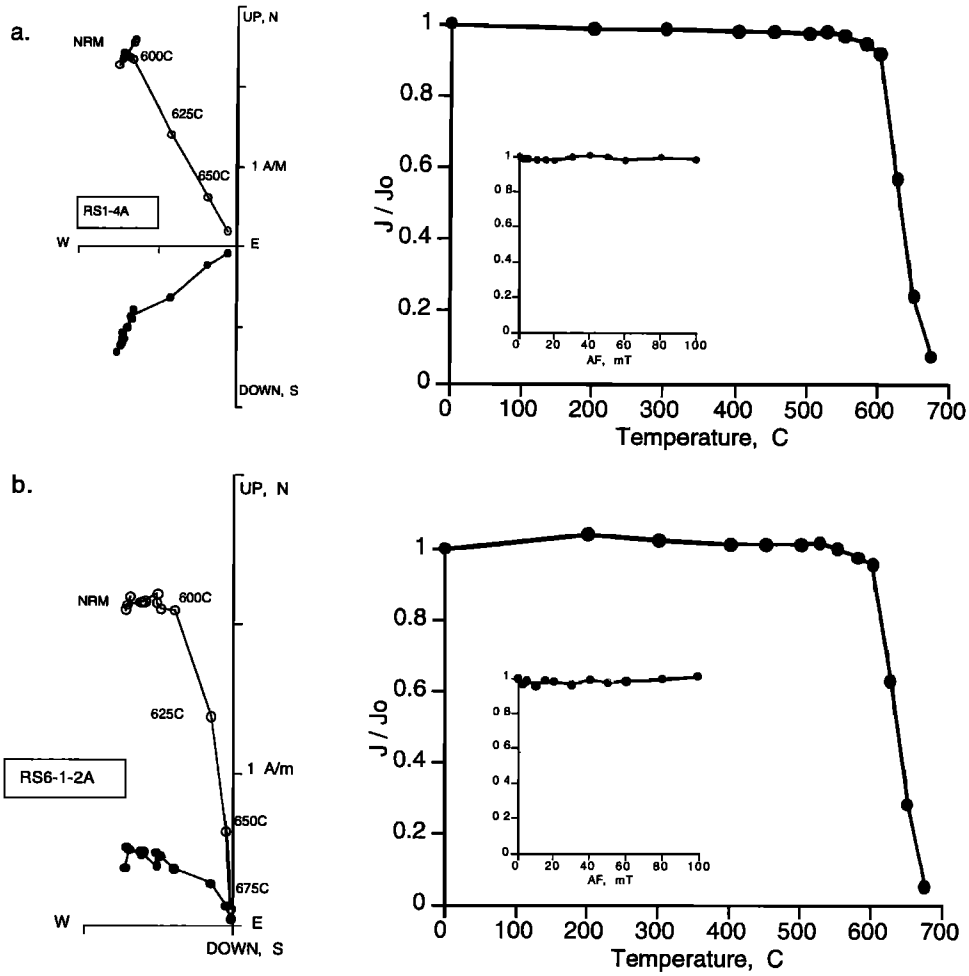

Figure 6. (left) Vector end-point diagrams and (right) normalized intensity plots for thermal demagnetization from 0 to 675°C for two samples, (a) RS1-4A and (b.) RS6-1-2A from the Russell Belt. On the demagnetization diagram open circles represent projections onto the E-W vertical plane, solid circles represent projections onto the horizontal plane. Insets in normalized intensity plots show normalized alternating field demagnetization on the same specimens.

between 600°C and 680°C, are attributed to Ti-poorer titanohematite.

5.7. Low Temperature SIRM

Low-temperature remanence measurements were made from 19 to 300 K with a Quantum Design (MPMS2) Squid magnetometer. Samples were cooled in a zero field to 19 K and given a saturation remanence in a field of 2.5 T, then measured in a near zero field at 5 K steps up to 300 K. For SIRM cooling experiments, a field of 2.5 T was applied at 300 K, then samples were cooled to 19 K. Remanence was monitored in a near zero-field with remanence measured every 5 K.

Low-temperature remanence measurements display a variety of features (Figure 11). Figure 11a shows cooling and warming curves for a titanohematite- and magnetite-bearing sample. In this sample a significant decay in remanence during cooling is observed around 250 K, where a Morin transition for hematite would be expected [*Morin*, 1950]. With continued cooling, remanence is unblocked at ~115 K, indicative of the Verwey transition (*Tv*), a cubic to monoclinic structural transition in magnetite [*O'Reilly*, 1984; *Moskowitz et al.*, 1998] or due to the magnetocrystalline anisotropy constant (K1) going to zero, which would cause a remanence loss in this temperature interval (100-120 K). Upon warming from 19 K, a small Néel transition for ferrian ilmenite is

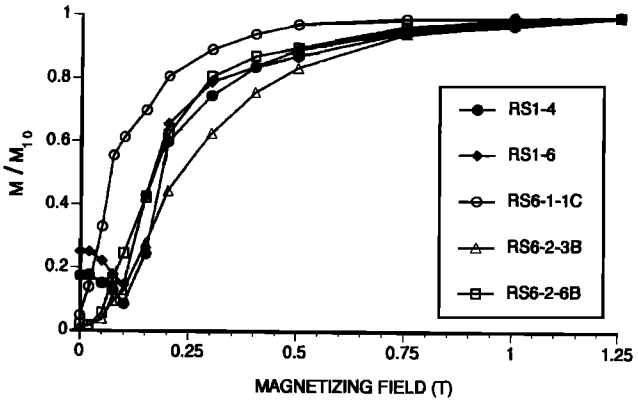

Figure 7. Plot showing isothermal remanent magnetization (IRM) normalized to magnetization at 1.25 T for five samples from the Russell Belt.

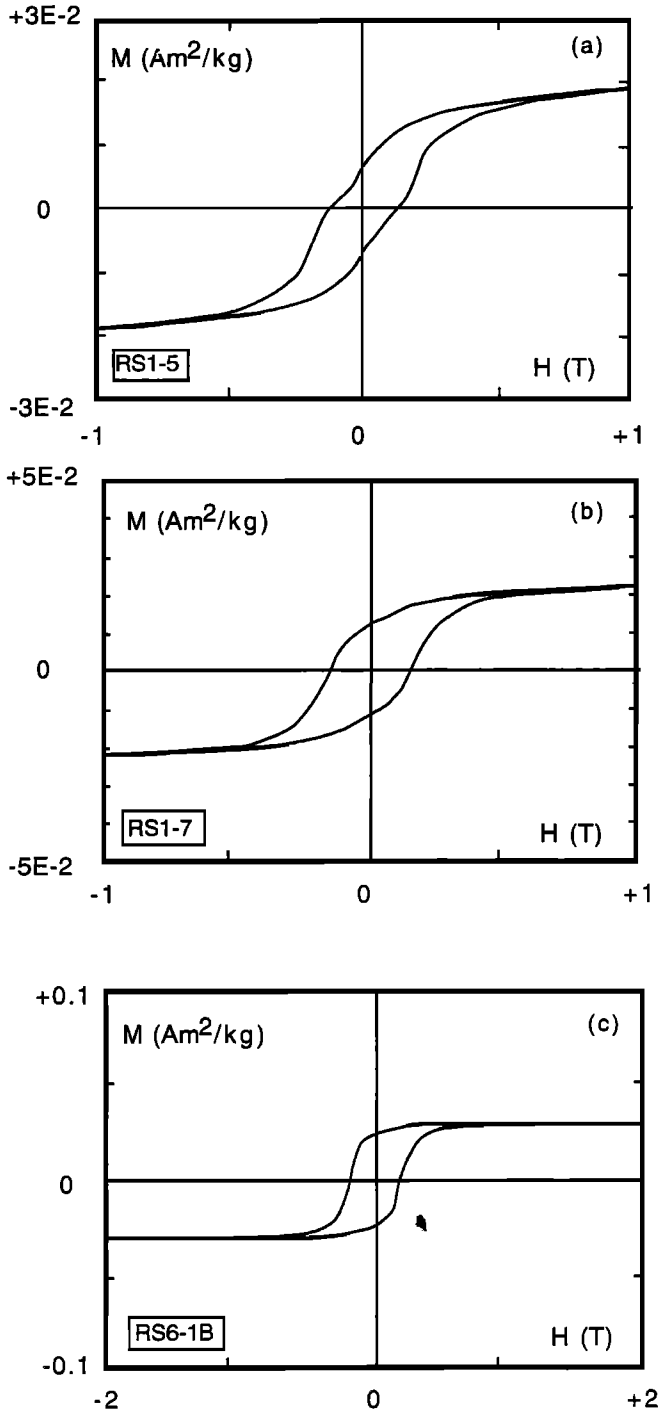

Figure 8. Hysteresis plots for three samples from the Russell Belt showing a variety of distinctive loops observed in these rocks, (a) "wasp-waisted," (b) "pot-bellied," (c) "hummingbird." Horizontal axis is applied field (H) in tesla; vertical axis is magnetization in Am^2/kg.

evident at ~60 K. With continued warming, remanence is lost both at ~110 and ~120 K as the sample warms through the Verwey transition for magnetite. Little change in remanence is observed above this temperature.

Figure 11b shows cooling and warming curves for sample RS1-7. Optical observations indicated only titanohematite as the magnetic oxide. During cooling experiments a very subtle Morin transition was observed at ~250 K (Figure 11b). The suppressed Morin transition may be due both to (1) the titanium content of the titanohematite host and (2) the very small grain size of the purer hematite lamellae within ilmenite lamellae. Compositionally, these lamellae would be purer than the host phase but well below the stable SD size limit for hematite. A Verwey transition was not observed in these samples. At very low temperatures the super paramagnetic hematite grains may be responsible for a small decrease in remanence. During warming, a very small loss in remanence at ~40 K is coincident with the Néel temperature for an iron-poor ferroilmenite [*Ishikawa and Akimoto*, 1957; *Banerjee*, 1991]. With continued warming to room temperature, little change in remanence was measured.

Figure 11c shows a third behavior observed with cooling to 19 K. A very small decay in remanence is observed at the Morin transition (~250 K, Figure 11c). With continued cooling, a distinct Verwey transition is observed at 115 K followed by little loss in remanence to 19 K. At the start of the warming experiment, there is a significantly larger remanence than at the start of the cooling SIRM. This increase is most likely due to the orientation of the sample. If the sample was coincidentally oriented such that the uniaxial axis was parallel to applied field, then at low temperatures a very large remanence would be obtained due to the alignment of the crystal while in the monoclinic state, a feature beautifully demonstrated by *Özdemir and Dunlop* [1999]. With warming from 19 K, a much larger loss in remanence occurred at the Verwey transition. Above the Verwey transition, little change in remanence was observed.

6. Summary and Discussion of Rock Magnetic Properties

The most remarkable property of the Russell samples is the large NRM with a mean value of 3.6 A/m, coupled

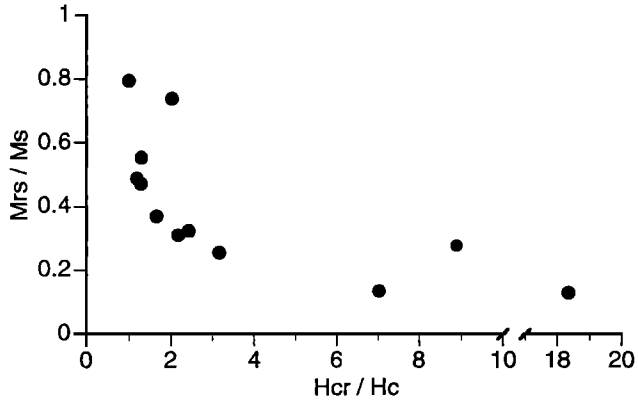

Figure 9. Plot of hysteresis parameter ratios for selected samples from the Russell Belt. Horizontal axis is the ratio of coercivity of remanence to coercive force. Vertical axis is ratio of saturation remanence to saturation magnetization. Note break in horizontal scale from 10 to 18.

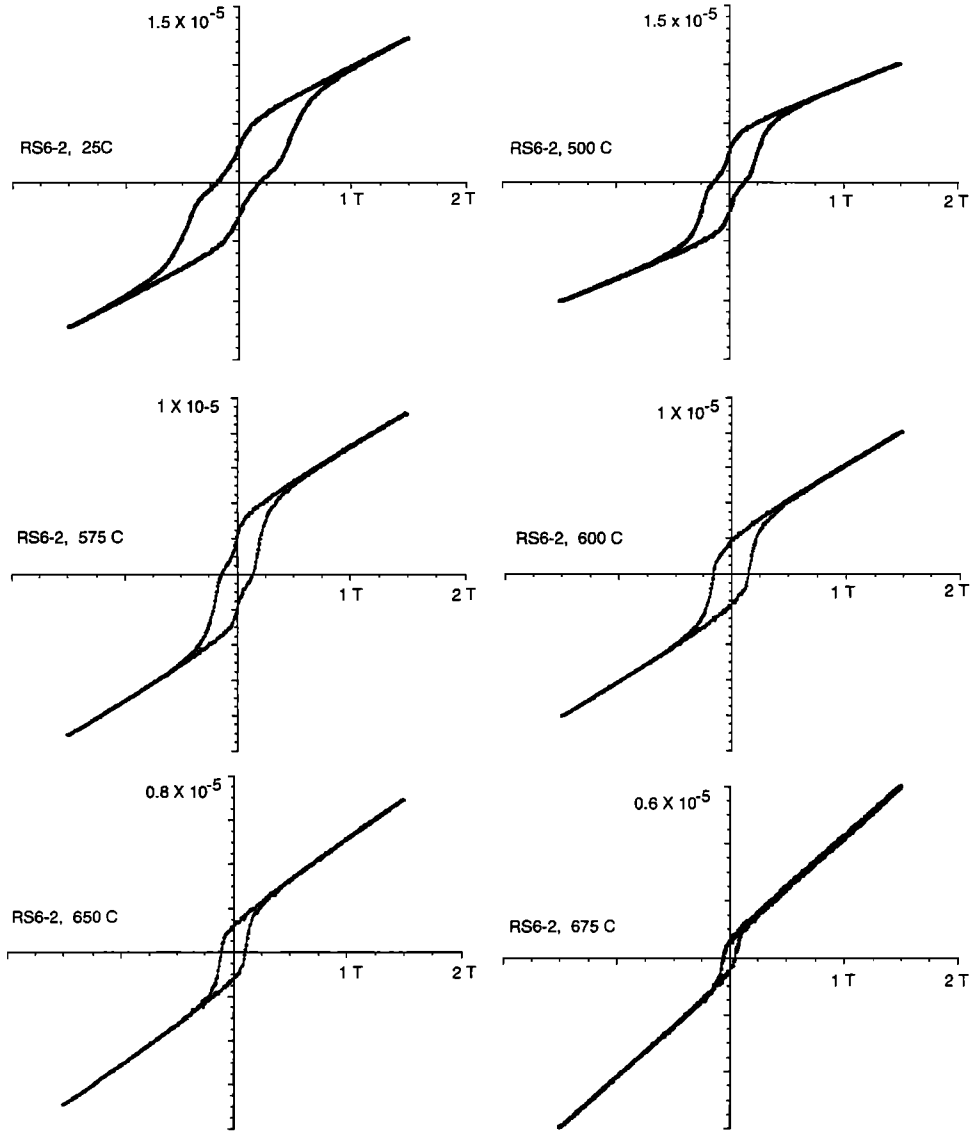

Figure 10. Diagram of hysteresis behavior for sample RS6-2 for temperatures of 25°C, 500°C, 575°C, 600°C, 650°C, and 675°C. Horizontal axis is applied field (*H*) up to 2 T. Vertical axis is magnetization (not corrected for slope).

with a very high coercivity. All samples were resistant to AF demagnetization with an average medium destructive field (MDF) above 100 mT. In contrast, the bulk susceptibility measurements were low with a bimodal distribution. Greater than 70% of the samples have susceptibility values less than 10^{-4} SI. As to other properties, two general types of behavior were found in the rock magnetic measurements. The differences in behavior are a function of mineralogy. One group has titanohematite + ilmenite + magnetite ± end-member hematite. The other has titanohematite + ilmenite ± end-member hematite.

Samples with a titanohematite + ilmenite + magnetite ± end-member hematite assemblage have thermal decay starting below 580°C but continuing to a maximum unblocking temperature of 670°C. NRM values ranged from $2x10^{-2}$ A/m to 9 A/m with an average of 3.6 A/m. They have average *Mrs/Ms* ratios of 0.3 and high *Hcr/Hc* values. These samples characteristically have wasp-waisted hysteresis loops, which change to lozenge shapes by 600°C. Verwey transitions, wasp-waisted hysteresis loops, and higher susceptibility values of up to 10^{-2} (SI) indicate the presence of magnetite. Magnetite is clearly contributing to the NRM, but in most samples, at least 90% of the NRM remains above 580°C, indicating that a majority of the NRM is carried by titanohematite-hematite.

Titanohematite + ilmenite ± hematite samples do not show a significant loss in magnetization until 600°C, with a maximum unblocking temperature of 670°C. This implies that the hematite contains less than 10% $FeTiO_3$, and there is no coexisting magnetite. These samples have NRM values up to 8.2 A/m, with an average value of 4 A/m. The average *Mrs/Ms* value is 0.55 and *Hcr/Hc* values are ≤ 2. Curie temperatures are above 600°C. Temperature hysteresis analyses show that hummingbird shape loops are retained up to 650°C. The lack of a Verwey transition and the low susceptibility values

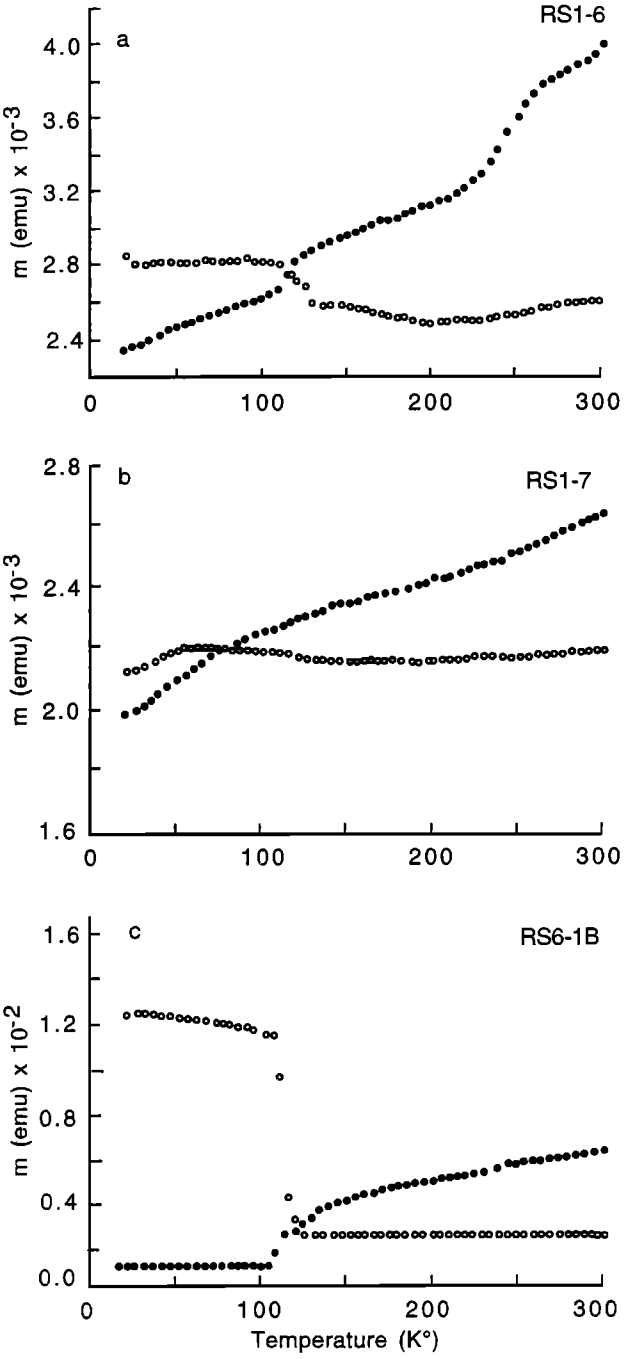

Figure 11. Saturation remanence acquired at 19 K and warmed to room temperature in a zero field (open circles) for samples (a) RS1-6, (b) RS1-7, and (c) RS6-1B. Also shown are saturation remanences acquired at room temperature and then cooled to 19 K in a zero field (solid circles). Distinct Verwey transitions are present in Figures 11a and 11c, and a Morin transition is present in sample RS1-6 (11a).

(averaging 10^{-4}SI) agree with the optical observations that magnetite is not part of the mineral assemblage. The saturation magnetization values and some NRM/SIRM ratios are high but are consistent with the mineralogy.

The rock magnetic data on the Russell samples clearly indicate that titanohematite is the predominant oxide and the primary remanence carrier. Though magnetite is present in some samples, its contribution is minor compared to the titanohematite, as clearly demonstrated by >90% of NRM remaining above 580°C. The high NRM intensities are explicable in terms of the known behavior of Ti-poor titanohematites, even though the maximum content of titanohematite in the rock is only 3%, because these compositions are very efficient carriers of thermoremanent and presumably thermochemical magnetization. *Uyeda* [1958] determined thermoremanent magnetization (TRM) susceptibilies of 170, 85, and 55 SI for 10 μm grains of reported compositions $hematite_{99}$, $hematite_{91}$, and $hematite_{83}$, respectively, in an applied field of 0.2 mT. Corresponding Koeningsberger ratios were 705, 336, and 770, respectively, comparable to the higher values obtained for the Russell Belt samples. *Syono et al.* [1962] obtained a TRM of 700 A/m in a field of 0.03 mT for a 5 mm × 5 mm × 1 mm MD crystal of pure hematite. *Clark* [1997] plots expected ranges for TRM intensity, chemical remanent magnetization (CRM) and corresponding Koeningsberger ratios for SD hematite and MD hematite based on these published experimental data and theoretical considerations. These data in Table 2 are compatible with the known properties of hematite and Ti-

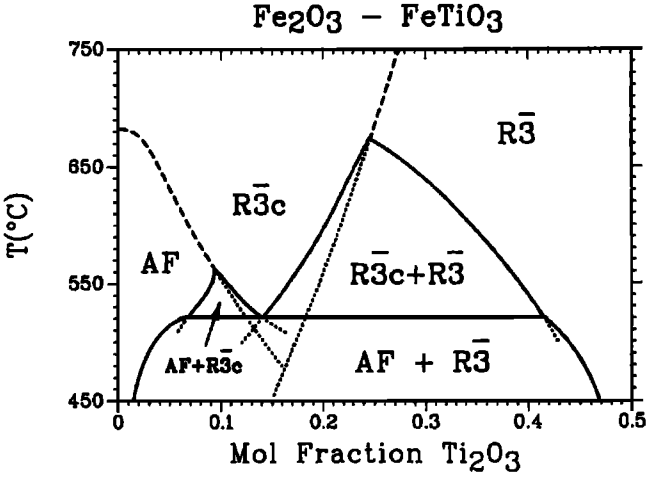

Figure 12. Calculated phase diagram of *Burton* [1991] for the ilmenite-hematite (Fe_2O_3-$FeTiO_3$) system. Compositions are expressed in mole fractions of 0% to 50% $Ti_2O_3/(Ti_2O_3+Fe_2O_3)$, where 50% corresponds exactly to $FeTiO_3$. The diagram shows three different two-phase regions. At the highest temperature on the right is the region of $R\bar{3}$ Ti-ordered ilmenite and $R\bar{3}c$ Ti-disordered titanohematite which closes upward at a tri-critical point on the $R\bar{3}c \rightarrow R\bar{3}$ Ti ordering phase transition. At intermediate temperatures on the left is the region of $R\bar{3}c$ Ti-disordered titanohematite and antiferromagnetically (AF) ordered (but Ti-disordered) hematite. At low temperatures the $R\bar{3}c$ phase is not stable, and there is a region of $R\bar{3}c$ Ti-ordered ilmenite and antiferromagnetically (AF) ordered hematite. This diagram does not illustrate the common ferrimagnetism of metastable $R\bar{3}$ Ti-ordered ilmenite with the compositions between 0.25 and 0.45. Possibilities for either a ferrimagnetic Ti-ordering ($R\bar{3}$) or antiferromagnetic (AF) ordering for a metastable $R\bar{3}c$ phase below 520°C are implied.

poor titanohematite. The greater stability of the NRM reflects the microstructure of the titanohematite grains. Ilmenite exsolution down to the nanometer scale in titanohematite has been found in comparable slowly cooled granulite rocks in southern Sweden [*Harrison et al.*, 1998]. It is probable that the Adirondack granulite rocks, produced during similar petrological conditions, also have these ultrafine exsolution features, which produce lamellae in the stable single-domain-size range. Phase coupling between the host and very fine exsolution products may also play a role. The interface between the host phase and ilmenite lamellae would be a region of high strain and mechanically could produce a region of higher coercivity and remanence intensity, yet retaining the magneto-chemical properties of those compositions. Such processes are not predicted for a single phase, but could be important where a single phase has undergone decomposition into two (or more) phases. Another unknown factor possibly related to the remanence could be the lamellae rich in pyrophanite component ($MnTiO_3$). Based on the experiments of *Ishikawa and Akimoto* [1958a,b], the contribution of this phase to the total titanohematite magnetic moment is probably minor.

Though many aspects of the rock magnetic data are consistent with titanohematite as the primary magnetic mineral, which is in good agreement with the low susceptibility values, mineral chemistry, and observed oxide mineralogy, there remains the problem that the average hematite mineral composition, $hematite_{83}$, should have lower unblocking and Curie temperatures than those measured. As discussed earlier, the titanohematite host mineral analyses may represent overlap analyses within a region of very fine two-phase exsolution. According to the Burton phase diagram (Figure 12) [*Burton*, 1991], these two phases could be a titanohematite, approximately $hematite_{71}$ with a disordered $R\bar{3}c$ structure and an antiferromagnetically (AF) $R\bar{3}$ ordered Ti-poor titanohematite, approximately $hematite_{86}$. Future transmission electron microscope (TEM) studies will explore this possibility.

Balsley and Buddington [1954] concluded that titanohematite was the major oxide and magnetic carrier. They surmised that the negative NRM directions might be due to self-reversals and considered *Néel's* [1951] theory that the reversed magnetization was due to a compact mixture of two materials with distinct Curie points "with the lower Curie point (material) ... magnetized opposite to the externally applied field by action of the demagnetizing field to the other constituent." *Balsley and Buddington* [p. 180, 1954]. We do not believe these samples have a self-reversed TRM as thought by *Balsley and Buddington* [1954] and also proposed for the Allard Lake samples [*Hargraves*, 1959; *Carmichael*, 1959]. This is because (1) the thermal directional decay of samples that contain titanohematite + hematite + magnetite and those with only titanohematite + hematite assemblages are indistinguishable and (2) the remanent vector is similar to other coeval rocks in the Adirondacks, which have a TRM carried only by magnetite. However, we do agree that the high NRM intensities may be due to a compositional effect and phase coupling in the very fine lamellae, allowing the ilmenite-richer compositions with short range ordering to have a high magnetic saturation and to have an abnormally high demagnetization temperature considerably above room temperatures.

It is possible that there may be an increased saturation effect in the hematite due to a ferrimagnetic ilmenite exsolving out of antiferromagnetic hematite. Based on the mineral compositional data, most of the bulk compositions would have initially intersected the AF + $R\bar{3}c$ two-phase field near the tricritical point [*Burton*, 1991]. At much lower temperatures the effect of a ferrimagnetic-antiferromagnetic phase-coupling could lead to an increase in magnetic saturation. If the compositional data at $hematite_{83}$ is correct, and not an overlap of analyses between ultrafine lamellae, then some of the $hematite_{83}$ could remain a mixed solid of an intermediate composition due to the sluggishness of diffusion at lower temperature and could cool metastably down to the $R\bar{3}c \rightarrow R\bar{3}$ ordering reaction, where it could become ferrimagnetic at low temperatures.

7. Titanohematite Contribution to the Russell Magnetic Anomaly

Magnetite is commonly assumed to be the predominant magnetic mineral in metamorphic terranes and, in particular, in granulite-facies rocks [*Mayhew et al.*, 1991]. Fundamental to this assumption is that induced magnetization will dominate the remanent magnetization, unless the magnetite is in the single-domain state. The magnetic response from multidomain magnetite would be that of induced magnetization, plus a subordinate, subparallel viscous component, and the rocks would have low Q values. Obviously this is not the situation in the Russell area, where a negative anomaly of 2250 nT is produced over this unit. It is worthwhile to examine the parameters that produce either a dominantly induced or remanent magnetic signature. When evaluating magnetic anomalies, NRM and susceptibility values are the two most important magnetic parameters. From these two parameters the Koenigsberger ratio (Q value) is calculated by dividing the NRM by the induced magnetization (susceptibility x ambient field). For our calculations we used a value of 58,000 nT (corresponding to a magnetizing force of 46.2 A/m) for the local magnetic field.

In areas where Q values are <1, the magnetic response mainly arises from the induced magnetization of the rocks, and areas with Q values >1 the remanent magnetization, i.e., the magnetization remaining after removal of an applied field, is the dominant contributor to the anomaly, provided the remanence directions are reasonably consistent. Where $Q > 10$ and NRM directions are consistent, the NRM overwhelmingly dominates the magnetic response of the rock, far exceeding the induced response. Of the Russell samples, 70% have Q values >10. Furthermore NRM directions are well grouped. In Figure 13, NRM and susceptibility values are plotted against Q values to show the relative contributions of susceptibility and remanence. As shown on Figure 13a, there is a wide variation in NRM values with more than half the samples having NRMs >3 A/m, and of these, 2/3 have values >6 A/m. In contrast, 92% of the samples have susceptibility values $<10^{-3}$ (SI). The low

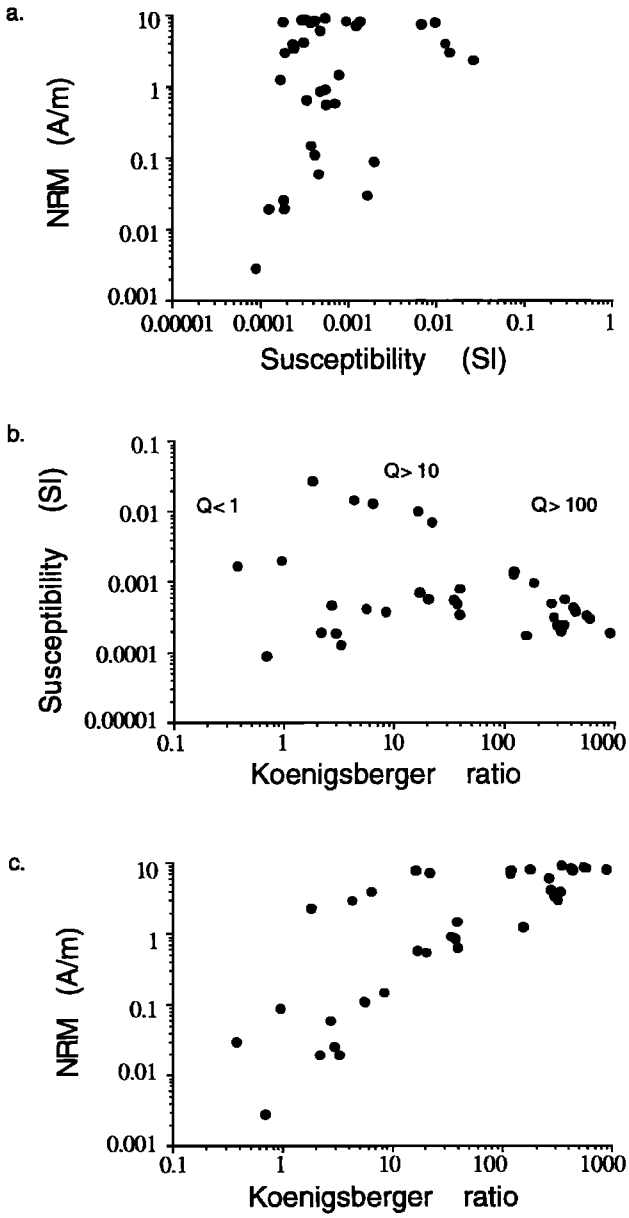

Figure 13. Plots of magnetic properties for samples from the Russell belt: (a) Log-log plot of susceptibility (SI units) versus natural remanent magnetization (NRM) in A/m. (b) Log-log plot of Koenigsberger ratio (Q) versus susceptibility (SI units). (c) Log-log plot of Koenigsberger ratio (Q) versus natural remanent magnetization in A/m. Dashed lines enclose data from the five samples that contain magnetite.

susceptibility values, on average 10^{-4}, are likely due to the abundance of ferric iron in the source rock prior to metamorphism, as most of the Fe in the samples is present as Fe_2O_3. Given these conditions, the high-coercivity mineral hematite or titanohematite is preferentially formed over magnetite. Other than titanohematite, there are only limited amounts of iron-bearing minerals in the mineral assemblage, and those are paramagnetic silicates. There is far less variation in susceptibility values than NRM values. The samples with susceptibility values $>10^{-2}$ have a small amount of discrete magnetite as part of the assemblage. There is little change in susceptibility with increasing Q values (Figure 13b), especially when the five samples known to contain discrete magnetite are eliminated. In contrast, when we evaluate the relationship between Q and NRM values (Figure 13c), a linear trend of increasing NRM with increasing Q values becomes evident. Again, when we exclude the samples known to contain discrete magnetite, we have an excellent correlation between NRM and Q value. These plots show that it is the high NRM values, rather than low susceptibilities, that significantly contribute to the very high Q values. The range in NRM values is a function of titanohematite content: the samples with higher contents yield higher NRM and Q values. Assuming the sample collection is representative of the distribution of magnetic properties in the gms unit, rigorous estimation of the average remanent magnetization of the unit, allowing for variations in the NRM directions, entails calculation of the vector mean NRM (sum of NRM vectors/number of vector). The result (Table 2) is NRM = 3.5 A/m, D = 258°, I = -59°. The maximum vertical magnetic anomaly associated with a vertical magnetization contrast M at a geological contact is $\mu M/_2$. The above NRM corresponds to an anomaly of ~1990 nT, consistent with the observed aeromagnetic anomaly (assuming that the magnetizations of adjacent units are much smaller than gms). Site to site variations of several amperes per meter in magnetizations can account for the local field variations in the ground magnetic profile of Figure 2b.

8. Implications for Modeling Anomalies

Few modern detailed studies exist on remanence-dominated anomalies [*Kelso et al.*, 1993; *Kletetschka and Stout*, 1998; *McEnroe et al.*, 1996, 2000]. In magnetic studies of deep crustal rocks it is generally assumed that high magnetizations are restricted to rocks with magnetite [*Shive et al.*, 1992]. *Frost* [1991] considers magnetite as the stable magnetic phase under high prograde metamorphic conditions. *Shive et al.* [1988] concluded that remanent magnetization contributes far less than the induced magnetization and that the total magnetization is not significantly greater than the induced magnetization. Fundamental to this conclusion is that if magnetite is the dominant magnetic mineral at depth, then the induced magnetization should predominate over remanent magnetization, unless magnetite is in the single-domain state. In either case, magnetite-bearing assemblages would have a Curie isotherm at ~580°C, or below, neglecting minor pressure effects. Unfortunately, many studies on deep crustal rocks have relied solely on rock magnetic techniques to determine the magnetic phases, even though many rock-magnetic properties are not unique. Future work needs to incorporate careful microscopy and microanalyses with the rock magnetic measurements. Given these assumptions, it is increasingly important to have rock magnetic data from sources that are not dominated by magnetite.

In studies on high-grade metamorphic rocks from the Adirondacks, northern Norway, and southern Sweden, titanohematite has been shown to retain high NRM values of the order necessary to produce strong anomalies. In

granulite samples from southwest Lofoten, northern Norway, *Schlinger and Veblen* [1989] showed that fine exsolution in coarse-grained titanohematite grains gave rise to very high coercivity and hysteresis properties similar to those of single-domain size crystals by inhibiting either (1) domain wall movement or (2) domain wall nucleation. These granulites have very high coercivities and unblocking temperatures up to 645°C. These properties are very similar to titanohematite-bearing granulites from southern Sweden that have very high NRM values, coercivities and unblocking temperatures [*McEnroe*, 1997]. These observations could have important implications for the interpretation of anomalies, especially in granulite-facies rocks where titanohematite can be an accessory mineral. Titanohematite-hematite is rarely considered as a contributor to short- or long-wavelength anomalies, but based on its properties of high NRM, coercivity, and stability to temperatures above that of magnetite, it should be seriously considered. In addition, the thermal relaxation conditions of hematite as displayed by *Pullaiah et al.* [1975] are more conducive to retaining remanence at higher temperatures over longer spans of geological time. The high NRM values, coercivities, and Q values are also found in slowly cooled igneous rocks containing members of the hematite-ilmenite solid solution series [*Carmichael*, 1959, 1961; *Hargraves*, 1959; *McEnroe*, 1995; *McEnroe et al.*, 1996, 2000]. All of these data show that remanence should be considered more fully when analyzing anomalies. Given the high coercivity and magnetization properties of titanohematite, it should also be considered as a possible source for magnetic anomalies on other planets.

9. Conclusions

The large negative magnetic anomaly produced by the Russell Belt gneiss arises from the strong reversed natural remanent magnetization of the rock, which dominates the induced magnetization that is associated with the relatively low susceptibilities. Optical and microprobe investigations indicate that titanohematite is the predominant magnetic oxide present, with only rare observations of scarce magnetite. The highly exsolved titanohematite has a typical bulk composition for the host phases of approximately $hematite_{83}$. It commonly has very fine-grained exsolution of ilmenite, pyrophanite, rutile, spinel ± corundum, and sulfides. Magnetic property measurements support titanohematite as the predominant magnetic carrier. Alternating field and thermal demagnetization studies, IRM measurements, hysteresis properties, and hysteresis behavior at temperature all indicate the dominance of this high-temperature, high-stability magnetic phase. Although the effects of composition and microstructure of titanohematite on NRM intensity and stability are not completely understood, it is important to consider titanohematite-hematite as a possible major contributor to magnetic anomalies worldwide. Titanohematite should be considered more fully when analyzing short- and long-wavelength anomalies, especially from deep crustal rocks, such as granulites, where this may be a more common phase than previously thought.

Acknowledgments. This work was encouraged by R. Hargraves, who generously donated original samples and field notes of A. F. Buddington. We thank Mike Jackson, Jim Marvin, and Peat Solheid of the Institute of Rock Magnetism, University of Minnesota, for help with the rock magnetic experiments and Bruce Moskowitz for guidance and discussions during and after our visit. We thank Peter Robinson for discussions on the silicate and oxide mineralogy and the metamorphic petrology. His comments were invaluable. We also thank Stephen Haggerty for discussions on oxide mineralogy and Mike Jercinovic for his super help with the microprobe facilities at UMass. None of the above individuals are responsible for our interpretations. Reviews by Mark Pilkington and Dave Clark greatly improved this manuscript. An NSF grant to McEnroe and support from the Geological Survey of Norway, Strategic Research Fund, supported this research. Support for the IRM is provided by grants from the Keck Foundation and the National Science Foundation.

References

Balsley, J.R., Total aeromagnetic intensity and geologic map of the Stark, Childwold and part of Russell quadrangles, N. Y., *U.S. Geol. Surv. Geophys. Invest. Map, GP 117*, 1954.

Balsley, J.R., and A.F. Buddington, Correlation of reversed remanent magnetism and negative anomalies with certain minerals, *J. Geomagn. Geoelectr., 6*, 176-181, 1954.

Balsley, J.R., and A.F. Buddington, Remanent magnetism of the Russell Belt of gneisses, northwest Adirondack Mountains, New York, *Adv. in Phys., 6*, 317- 322, 1957.

Balsley, J.R., and A.F. Buddington, Iron titanium oxide minerals, rocks, and aeromagnetic anomalies of the Adirondack area, New York, *Econ. Geol., 53*, 777-805, 1958.

Banerjee, S.K., New grain size limits for paleomagnetic stability in hematite, *Nature Phys. Sci., 232*, 15-16, 1971.

Banerjee, S.K., Magnetic properties of Fe-Ti oxides, in *Oxide Minerals: Petrologic and Magnetic Significance, Rev. Mineral.*, vol. 25,edited by D.H. Lindsley, pp. 107-128, Mineral. Soc. of Am., Washington, D.C., 1991.

Blakely, R.J., *Potential Theory in Gravity and Magnetic Applications*, 441 pp., Cambridge Univ. Press, New York, 1996.

Bohlen, S.K., J. W., Valley, and E. Essene, Metamorphism in the Adirondacks, I, Petrology, pressure, and temperature, *J. Petrol., 26*, 971-992, 1985.

Books, K.G., Remanent magnetism as a contributor to some aeromagnetic anomalies, *Geophysics, 27*, 359-375, 1962

Bozorth, R.M., D.E. Walsh, and A.J. Williams, Magnetization of ilmenite-hematite system at low temperatures, *Phys. Rev., 108*, 157-158, 1957.

Buddington, A.F., Adirondack igneous rocks and their metamorphism, *Mem. Geol. Soc. Am., 7*, 354 pp., 1939.

Buddington, A.F., and B.F. Leonard, Regional geology of the St. Lawrence County magnetite district, northwest Adirondacks, New York, *U.S. Geol. Surv. Prof. Pap., 376*, 145 pp., 1962.

Burton, B.P., The interplay of chemical and magnetic ordering, in *Oxide Minerals: Petrologic and Magnetic Significance, Rev. Mineral.*, vol. 25, edited by D.H. Lindsley, pp. 303-321, Mineral. Soc. of Am., Washington, D.C, 1991.

Carmichael, C.M., Remanent magnetism of the Allard Lake ilmenite, *Nature, 183*, 1239-1241, 1959.

Carmichael, C.M., The magnetic properties of ilmenite-hematite crystals, *Proc. R. Soc. London, Ser. A, 263*, 508-530, 1961.

Clark, D.A., Magnetic petrophysics and magnetic petrology: Aids to geologic interpretation of magnetic surveys, *J. Aust. Geo. Geophys., 17*, 83-103, 1997.

Clark, D.A., Magnetic petrology of igneous intrusions: implications for exploration and magnetic interpretation, *Ex. Geophys., 30*, 5-26, 1999.

Dunlop, D.J., and O. Özdemir, *Rock Magnetism: Fundamentals and Frontiers*, 573 pp., Cambridge Univ. Press, New York, 1997.

Frost, B.R., Magnetic petrology: Factors that control the occurrence of magnetite in crustal rocks, in *Oxide Minerals: Petrologic and Magnetic Significance, Rev. Mineral.*, vol. 25,

edited by D.H. Lindsley, Mineral. Soc. of Am., Washington, D.C., pp. 489-506, 1991.

Grant, F.S., Aeromagnetic, geology and ore environments, I, Magnetite in igneous, sedimentary and metamorphic rocks: An overview, *Geoexploration, 23*, 303-333, 1985.

Green, R., Remanent magnetization and the interpretation of magnetic anomalies, *Geophys. Prospect., 8*, 98-110, 1960.

Hargraves, R.B., Magnetic anisotropy and remanent magnetization in hemo-ilmenite from ore deposits of Allard Lake Quebec, *J. Geophys. Res., 64*, 1565-1573, 1959.

Harrison, R., U. Golla, S. McEnroe, and A. Putnis, The effect of ultra fine-scale exsolution lamellae on the magnetic properties of the ilmenite-hematite solid solution: Microstructural and chemical investigation using energy-filtered TEM, *Electron Microscopy*, Symp. E, *1*, 233-234, 1998.

Hoffman, K.A., Self-reversal of thermoremanent magnetization in the ilmenite-hematite system: Order-disorder, symmetry, and spin alignment, *J. Geophys. Res., 97*, 10,883-10,895, 1992.

Ishikawa, Y., Electrical properties of $FeTiO_3$-Fe_2O_3 solid solution series, *J. Phys. Soc. Jpn., 13*, 37-42, 1958.

Ishikawa, Y., and S. Akimoto, Magnetic properties of $FeTiO_3$-Fe_2O_3 solid solution series, *J. Phys. Soc. Jpn., 12*, 1083-1098, 1957.

Ishikawa, Y., and S. Akimoto, Magnetic property and crystal chemistry of ilmenite ($MeTiO_3$) and hematite (αFe_2O_3) system, I, Crystal chemistry, *J. Phys. Soc. Jpn., 13*, 1110-1118, 1958a.

Ishikawa, Y., and S. Akimoto, Magnetic property and crystal chemistry of ilmenite ($MeTiO_3$) and hematite ($\alpha Fe_2 O_3$) system II. Magnetic property, *J. Phys. Soc. Jpn., 13*, 1298-1310, 1958b.

Ishikawa, Y., and Y. Syono, Order-disorder transformation and reverse thermo-remanent magnetism in the $FeTiO_3$-Fe_2O_3 system, *J. Phys. Chem. Solids, 24*, 517-528, 1963.

Kelso, P.R., S.K. Banerjee, and C. Teyssier, Rock magnetic properties of the Arunta Block, central Australia, and their implications for the interpretation of long-wavelength magnetic anomalies, *J. Geophys. Res., 98*, 15,987-15,999, 1993.

Kletetschka, G., and J.H. Stout, The origin of magnetic anomalies in lower crustal rocks, Labrador, *Geophys. Res. Lett., 25*, 199-202, 1998.

Leonard, B., and A. Buddington, Ore deposits of the St. Lawrence County magnetite district, northwest Adirondacks, New York, *U.S. Geol. Surv. Prof. Pap., 377*, 259 pp., 1962.

Lindsley, D.H., Experimental studies of oxide minerals, in *Oxide Minerals. Petrologic and Magnetic Significance,Rev. Mineral.*, vol. 25, edited by D.H. Lindsley, pp. 69-106, Mineral. Soc. of Am., Washington, D.C., 1991.

Mayhew, M.A., P.J. Wasilewski, and B.D. Johnson, Crustal magnetization and temperature at depth beneath the Yilgarn block, western Australia inferred from Magsat data, *Earth Planet. Sci. Lett., 107*, 515-522, 1991.

McEnroe, S. A., Paleomagnetic signatures and rock magnetic properties from rapidly uplifted high-pressure metamorphic rocks and intrusive igneous rocks in Sveconorwegian Orogen, Sweden, *Geonytt., 22*, 48, 1995.

McEnroe, S.A., Ilmenite mineral magnetism: implications for geophysical exploration for ilmenite deposits, *Nor. Geol. Surv. Bull., 433*, 36-37, 1997.

McEnroe, S.A., P. Robinson, and P. Panish, Rock-magnetic properties, oxide mineralogy, and mineral chemistry in relation to aeromagnetic interpretation and the search for ilmenite reserves, *Nor. Geol. Surv. Rep., 96.060*, 148 pp., 1996.

McEnroe, S.A., P. Robinson, and P. Panish, Detailed chemical characterization of ilmenite and magnetite compositions in oxide-rich cumulates of the Sokndal region, Rogaland, Norway, *Nor. Geol. Survey Bull.*, in press, 2000.

McLelland, J., Geochronology and petrogenesis of Adirondack igneous and metamorphic rocks, in *Field Trip Guidebook for the Northeastern United States*, edited by J.T. Cheney and J.C. Hepburn, Geological Society of America annual meeting, Contribution no. 67, Department of Geology and Geography, University of Massachusetts, Amherst, pp. J1-J29, 1993.

McLelland, J., J.S. Daly, and J.M. McLelland, The Grenville Orogenic cycle (ca. 1350-1000 Ma): An Adirondack perspective, *Tectonophysics, 265*, 1-29, 1996.

Mezger, K., C.M. Rawnsley, S.R. Bohlen, and G.N. Hanson, U-Pb garnet, sphene, monazite, and rutile ages: Implications for the duration of high-grade metamorphism and cooling histories, Adirondack Mts., New York, *J. Geol., 99*, 415-428, 1991.

Mezger, K., B. van de Pluijm, E. Essene, and A. Halliday, The Carthage-Colton mylonite zone (Adirondack Mountains, N.Y.): The site of a cryptic suture zone within the Adirondack orogen?, *J. Geol., 100*, 630-638, 1992.

Morin, F.J., Magnetic susceptibility of Fe_2O_3 and Fe_2O_3 with added titanium, *Phys. Rev., 78*, 819-820, 1950.

Moskowitz, B.M., M. Jackson, and C. Kissel, Low-temperature magnetic behavior of titanomagnetites, *Earth Planet. Sci. Lett., 157*, 141-149, 1998.

Nagata, T., S. Uyeda, and S. Akimoto, Self-reversal of thermo-remanent magnetization of igneous rocks, *J. Geomagn. Geoelectr., 4*, 22-38, 1952.

Néel, L., L'inversion de l'aimantation permanente des roches, *Ann. Geophys., 7*, 90-102, 1951.

Nord, G.L., and C.A. Lawson, Order-disorder transition-induced twin domains and magnetic properties in ilmenite-hematite, *Am. Mineral., 74*, 160-176, 1989.

Nord, G.L., and C.A. Lawson, Magnetic properties of $ilmenite_{70}$-$hematite_{30}$: Effect of transformation induced twin boundaries, *J. Geophys. Res., 97*, 10,897-10,910, 1992.

O'Reilly, W., *Rock and Mineral Magnetism*, 220 pp., Blackie, Glasgow, 1984.

Özdemir, Ö., and D.J. Dunlop, Low-temperature properties of a single crystal of magnetite oriented along principal magnetic axes, *Earth Planet. Sci. Lett., 165*, 229-239, 1999.

Özdemir, Ö., D.J. Dunlop, and B.M. Moskowitz, The effect of oxidation on the Verwey transition in magnetite, *Geophys. Res. Lett., 20*, 1671-1674, 1993.

Pullaiah, G., E. Irving, K. Buchan, and D. Dunlop, Magnetization changes caused by burial and uplift, *Earth Planet. Sci. Lett., 28*, 133-143, 1975.

Rajagopalan, S., D. Clark, and P. Schmidt, Magnetic mineralogy of the Black Hill Norite and its aeromagnetic and palaeomagnetic implications, *Exp. Geophys., 26*, 215-220, 1995.

Ramdohr, P., *The Ore Minerals and Their Intergrowths*, 1,174 pp., Pergamon, Tarrytown, N. Y., 1969.

Reford, M.S., Magnetic method, *Geophysics, 45*, 1640-1658, 1980.

Rumble, D., Oxide minerals in metamorphic rocks, in *Oxide Minerals, Short Course Notes, vol. 3*, edited by D. Rumble, pp. R1-R24, Mineral. Soc. of Am., Washington, D.C., 1976.

Schlinger, C., Magnetization of lower crust and interpretation of regional magnetic anomalies: Example from Lofoten and Vesteralen, Norway, *J. Geophys. Res., 90*, 11,484-11,504, 1985.

Schlinger, C., and D.R. Veblen, Magnetism and transmission electron microscopy of Fe-Ti oxides and pyroxenes in a granulite from Lofoten, Norway, *J. Geophys. Res., 94*, 14,009-14,026, 1989.

Shive, P.N., Can remanent magnetization in the deep crust contribute to long wavelength magnetic anomalies?, *Geophys. Res. Lett., 16*, 89-92, 1989a.

Shive, P.N., Reply, *Geophys Res. Lett., 16*, 599-600, 1989b.

Shive, P.N., B.R. Frost, and A. Peretti, The magnetic properties of metaperidotitic rocks as a function of metamorphic grade: Implications for crustal magnetic anomalies, *J. Geophys. Res., 93*, 12,187-12,195, 1988.

Shive, P., R.J. Blakely, B.R. Frost, and D.M. Fountain, Magnetic properties of the lower continental crust, in *Continental Lower Crust*, edited by D.M. Fountain, R. Arculus, and R.W. Kay, pp. 145-177, Elsevier Sci., New York, 1992.

Spear, F.S., and J.C. Markussen, Mineral zoning, P-T-X-M phase relations, and metamorphic evolution of some Adirondack granulites, New York, *J. Petrol., 38*, 757-783, 1997.

Syono, Y., S. Akimoto, and T. Nagata, Remanent magnetization of ferromagnetic single crystal, *J. Geomagn. Geoelectr., 14*, 113-124, 1962.

Thompson, R. and F. Oldfield, *Environmental Magnetism*, 227 pp., Allen and Unwin, Winchester, Mass., 1986.

Uyeda, S., Thermo-remanent magnetism as a medium of paleomagnetism, with special reference to reverse thermo-remanent magnetism, *Jpn. J. Geophys.*, *2*, 1-123, 1958.

Watkins, N.D. The relative contributions of remanent and induced magnetization to the observed field in northeast Alberta, *Geophys. Prospect.*, *9*, 421-426, 1961.

Westcott-Lewis, M.F. and L.G. Parry, Magnetism in rhombohedral iron-titanium oxides, *Aust. J. Phys.*, *24*, 719-734, 1971a.

Westcott-Lewis, M.F., and L.G. Parry, Thermoremanence in synthetic rhombohedral iron-titanium oxides, *Aust. J. Phys.*, *24*, 735-7342, 1971b.

Wiener, R. W., J.M. McLelland, Y.W. Isachsen, and L.M. Hall, Stratigraphy and structural geology of the Adirondack Mountains, New York: Review and synthesis, in *The Grenville Event in the Appalachians and Related Topics*, edited by M.J. Bartholomew, Spec. Pap. Geol. Soc. Am.*194*, 1-55, 1984.

Worm, H.-U., Comment on "Can remanent magnetization in the deep crust contribute to long wavelength magnetic anomalies?" by Peter N. Shive, *Geophys. Res. Lett.*, *16*, 595-597, 1989.

L.L. Brown, Department of Geosciences, University of Massachusetts, Amherst, MA 01003. (lbrown@umass.edu)

S. A. McEnroe, Norwegian Geological Survey, N-7491 Trondheim, Norway. (Suzanne.McEnroe@ngu.no)

(Received August 16,1999; revised December 23, 1999; accepted February 9, 2000)